Atmospheric Research 291 (2023) 106820

Contents lists available at ScienceDirect

Atmospheric Research

journal homepage: www.elsevier.com/locate/atmosres

The seasonal cycle of cloud radiative effects over Congo Basin based on CERES observation and comparison to CMIP6 models

A. Dommo [a,b,c,*], Nana Ama Browne Klutse [c,d], Stephanie Fiedler [e,1], Hubert Azoda Koffi [c], Derbetini A. Vondou [b]

[a] National Advanced School of Engineering, University of Yaoundé 1, Yaoundé, Cameroon
[b] Laboratory of Environmental Modeling and Atmospheric Physics, University of Yaoundé 1, Yaoundé, Cameroon
[c] Department of physics, University of Ghana, Accra, P.O. Box LG 63, Ghana
[d] African Institute of Mathematical Sciences (AIMS), Sector Remera, Kigali 20093, Rwanda
[e] University of Cologne, Institute of Geophysics and Meteorology, Cologne, Germany

ARTICLE INFO

Keywords:
Central Africa
Cloud radiative effect
CMIP6
CERES

ABSTRACT

This study investigates the seasonal variability of the cloud radiative effects (CREs) over Congo Basin (CB) using 15-year observations from Clouds and the Earth's Radiant Energy System (CERES) Energy Budget and Filled (EBAF) Ed4.1 level 3b dataset involving CERES and Moderate Resolution Imaging Spectroradiometer (MODIS) instruments on board Terra and Aqua satellites. The relationships between CREs and cloud properties such as total cloud fraction (TCF), cloud top height (CTH), cloud top temperature (CTT) and cloud optical thickness (COT) are checked. An evaluation of Coupled Model Intercomparison Project (CMIP) Phase 6 in capturing the seasonal cycle of CREs as well as the magnitudes of the CREs along the seasonal cycle is also performed. This study shows a net cloud cooling effect of -8.4 W/m^2 and $-$ 43.9 W/m^2 respectively at the top of the atmosphere (TOA) and at the surface, leading to a net warming effect of 35.67 W/m^2 in the atmosphere. This value implies a large energy source over the Central Africa (CA) atmospheric column. The associated relationships between CREs and cloud properties show that the shortwave CRE is more sensitive to TCF and optical thickness whereas its longwave counterparts is more sensitive to CTH, CTT and COT at the TOA and in the atmosphere. All of the four CMIP6 models used in this study can capture the spatial pattern of CREs as well as their seasonal cycle but misrepresent intensity of CREs. Results also show that a better-simulated TCF considerably reduces the intensity of the annual mean underestimation in both longwave and shortwave CRE for some CMIP6 models, but not for models with overestimated shortwave CRE.

1. Introduction

Central Africa (CA) is a region encompassing the second largest forest in the world, which acts as a carbon sink and influences the global climate system (Baccini et al., 2012; Dargie et al., 2017). This region is understudied because of the typical lack of data, yet the regional climate needs to be better understood. For instance the regional clouds, precipitation and circulation are not yet well elucidated although considerable progress are noticeable (Pokam et al., 2011, 2014; Taguela et al., 2020; Kuete et al., 2019, 2022; Tamoffo et al., 2021, 2022; Taguela et al., 2022a, 2022b; Moihamette et al., 2022). Precipitation, clouds, and circulation remain poorly represented in climate models (Bony et al., 2015; Jiang et al., 2013; Lauer and Hamilton, 2013), and may contribute to model differences in the energy budget.

At the top of the atmosphere (TOA), the measurement of the energy budget has been possible thanks to satellite observations (Chen et al., 1996; Chen et al., 2000; Johnson et al., 1999; Hartmann et al., 2001). Using the observations from the International Cloud Climatology Project (ISCCP) Hartmann et al. (2001) showed that over tropical convective regions, individual clouds can have positive or negative effects on the radiation budget. For instance, Cirrus clouds are recognized for their unique effect on radiative fluxes (Liou, 1992). Whereas most cloud types warm the atmosphere and the surface at night, Cirrus is the only cloud type that can warm or cool the daytime atmosphere and surface

* Corresponding author.
E-mail address: dmmatanas@gmail.com (A. Dommo).
[1] Now: GEOMAR Helmholtz Centre for Ocean Research Kiel & Faculty of Mathematics and Natural Sciences, Christian-Albrechts-University of Kiel, Kiel, Germany.

https://doi.org/10.1016/j.atmosres.2023.106820
Received 17 February 2023; Received in revised form 11 May 2023; Accepted 17 May 2023
Available online 25 May 2023

depending on the physical characteristics such as cloud height, temperature, liquid water path, and optical thickness (Stephens and Webster, 1981). Using Earth Radiation Budget experiment (ERBE) and ISCCP data in conjunction with radiative transfer model to estimate the effect of various cloud types at the TOA, Hartmann et al. (2001) showed that the overall effect (positive and negative) of the ensemble of clouds at the TOA nearly cancel over the tropics. Similar results have been seen earlier by regressing data from the ERBE onto ISCCP (Ramanathan et al., 1989; Harrison et al., 1990; Hartmann et al., 1992). Generally defined as the energetic forcing due to cloud, cloud radiative effect (CRE) is strongest at the surface through its shortwave component, whereas its longwave counterpart is strongest in the atmosphere (Collins et al., 1996).

Clouds increase the downwelling longwave (LW) radiation flux in the atmosphere and also reflect incoming shortwave (SW) radiation back to space. However, despite its importance on atmospheric circulation (Peixoto, 1992; Watt-Meyer and Frierson, 2017), there is no consensus about the net atmospheric CRE at the global scale. Some studies showed a strong net cloud cooling effect (Stephens et al., 2012) in response to SW cooling dominating the LW warming, whereas others exhibit a net warming effect mostly due to a comparably small SW cloud cooling effect (Wild et al., 2014, 2018) if not zero (Kato et al., 2018). This lack of consensus demonstrates the challenge of accurately quantifying the net effect of clouds in the atmosphere. The surplus of energy in the tropics leads to a net energy transport to the extra-tropics by the meridional circulation (Peixoto, 1992). Thus, the CRE in the tropics with the implications for the atmospheric circulation motivates our interest in quantifying the amount and the variability of the CRE over CA.

At the surface, clouds exert a strong influence on the energy budget through their effect on LW and SW radiation. Generally, clouds radiatively warm the surface by absorbing and reemitting terrestrial thermal emission that would otherwise escape the earth system. They also cool the surface by reflecting the downward solar radiation back to space that would otherwise be absorbed by the surface. The combination of the two competing effects is called the CRE, which defines the changes in LW and SW radiation budget in the presence of clouds. At the global scale, it is known that clouds radiatively cool the Earth's surface and the magnitude of cooling ranges between 20 and 25 W/m^2 (Kato et al., 2018; L'Ecuyer et al., 2019) with the SW cooling dominating the LW warming at least by a factor two, except in some areas such as the polar regions where LW warming can be larger than the SW cloud cooling effect (Garrett and Zhao, 2006; Henderson et al., 2013; Zhao and Garrett, 2015). Most of the radiative energy absorbed at the surface is converted into latent and sensible heat flux (Stephens et al., 2012; Wild, 2012a, 2012b; Wild et al., 2012, 2014, 2018) and another part is reemitted by the surface as thermal radiation that heats the atmosphere. The measurement of the surface energy balance is relatively much more complex, and cannot be done directly from space, because of the interactions with the atmospheric constituents that modulate the signals of the terrestrial flux emitted or reflected back to satellite sensors. Thus, large biases have been recorded on the shortwave radiation at the Earth's surface (Rossow and Zhang, 1995; Li et al., 2013). These biases are seen in many global climate models which struggle to realistically represent the energy balance at the Earth's surface (Wild et al., 2012, 2014). As a consequence of the coupling of the energy and water cycle, also our knowledge on the intensity of the water cycle is limited. At the surface, the hydrological cycle is fed by the surface radiative balance which provides energy in the form of latent and sensible heat flux which are necessary for evapotranspiration (Stephens et al., 2012; Wild, 2012b). Therefore, knowing the seasonal variability of CRE may help to better understand the hydrological cycle in CA, and consequently the causes of rainfall variability over the region.

The energy budget is a fundamental determinant for the climate and has a direct influence on atmospheric circulation. For instance, some studies (Tompkins, 2005; Rodwell and Jung, 2008) showed that circulation and precipitation differences over West Africa arise from the direct radiative effect of aerosol changes, based on the European Centre for Medium-RangeWeather Forecasts (ECMWF) model. In the Met Office Unified Model, the strength of the West African Monsoon (WAM) is also affected by changes to clouds and hence radiation (Marsham et al., 2013; Birch et al., 2014). More recently, Li et al. (2014) highlighted a strong sensitivity of the WAM circulation and associated precipitation to the radiation schemes used in their simulations. Clouds play a major role in regulating the energy imbalance (Ramanathan et al., 1989; Curry et al., 1996; Shupe and Intrieri, 2004; Xie et al., 2013) which is important for regional climate variability, as it influences local atmospheric circulation (Watt-Meyer and Frierson, 2017) and sea surface temperature (Li et al., 2020a, 2020b). For instance, the coupling between CREs and atmospheric circulation leads to increases in sea surface temperature variability on time scales longer than a month throughout the tropical oceans. Watt-Meyer and Frierson (2017) argued that the responses of the atmospheric CRE on circulation include both equatoward and poleward shifts of the eddy-driven jet of varying magnitudes despite a strengthening of the Hadley cell in response to heating in the upper troposphere. CREs differ in global climate models, at least in parts due to the limited understanding of clouds and aerosols (Schulz et al., 2006; Myhre et al., 2012; Xie et al., 2013). Any perturbations in the simulated clouds, such as forced by aerosol-cloud interactions or through cloud feedbacks, can have a strong influence on the energy distribution in the climate system. According to the International Panel on Climate Change (IPCC) sixth assessment report (AR6), global warming acts to decrease the low clouds amount and therefore amplify the warming (Forster et al., 2021).

The aim of this work is to depict the effects of clouds on radiation over CA, based on satellite and model data. More precisely, we will evaluate the seasonality of the CREs over CA by also linking it with the sea surface temperature anomaly from the ERA5 reanalysis, compare the magnitude of CRE in CA to the global average, and investigate the dependencies of CRE on cloud properties using satellite data from CERES (Loeb et al., 2018). In a second step, we use the gained insights for an evaluation of CRE in four models in the Coupled Model Intercomparison project phase 6 (CMIP6, Eyring et al., 2016). Our CRE analysis is performed for the TOA, in the atmosphere and at the surface. This work is organized as follows: section 2 describes the data and the methods used in this study, section 3 describes the spatial pattern and seasonal cycle of CREs over CA. Section 4 looks at the associated relationships between CREs and the clouds properties and section 5 present the evaluation of CMIP6 models. The article ends with a discussion and conclusion in section 6.

2. Data and methods

2.1. Data

2.1.1. CERES

The Clouds and the Earth's Radiant Energy System (CERES) Energy Budget and Filled (EBAF) (hereafter, CERES-EBAF) dataset is produced using measurements from several instruments (Loeb et al., 2018). It combines measurements from the CERES and MODIS instruments aboard the Terra and Aqua satellites with measurements from geostationary satellites that provide diurnal information. The TOA and surface radiative fluxes in this study are obtained from the CERES-EBAF Ed4.1 level 3b, which is the latest version of the CERES-EBAF dataset. Surface irradiances are computed with other products such as cloud and aerosol properties, temperature and specific humidity profiles. Surface irradiances might therefore be susceptible to potential errors from input data needed for computations. In order to reduce the error in the surface irradiances and increase the consistency with TOA fluxes, TOA irradiances are used to constrain the surface irradiances (Kato et al., 2013). The radiance to flux conversion is performed using empirical Angular Distribution Models (Su et al., 2015). The CERES-EBAF data provides a long term integrated global climate data record for detecting decadal changes

in Earth's Radiation budget (ERB) from the surface to the TOA, together with the associated cloud and aerosol properties. The dataset enables to improve the understanding of the variability in the radiation budgets and allows climate models evaluation to support further improvements. Past CERES products have been widely used for climate studies (Rutan et al., 2009; Stephens et al., 2012; Berry and Mace, 2014; Hill et al., 2016, 2018; Li et al., 2020a, 2020b) and for climate models evaluation (Xie et al., 2013; Wild et al., 2014, 2018; Loeb et al., 2020; Wild, 2020; Li et al., 2021, 2022). In our study, we use fluxes at the TOA and at the surface for clear and cloudy conditions with monthly resolution on a 1°x1° spatial grid to determine CREs. Cloud properties are taken from CERES-SYN1deg edition 4A, namely total cloud fraction (TCF), cloud top height (CTH), cloud top temperature (CTT) and cloud visible optical thickness (COT) over CA for the period March 2000–December 2014.

2.1.2. CMIP6

Output of the historical simulations from the Coupled Model Intercomparison Project Phase 6 (CMIP6, Eyring et al., 2016) are used in this study. Compared to CMIP5, spatial resolution and physical processes have changed with some clear improvements (Furtado et al., 2015; Eyring et al., 2016; Kay et al., 2016). A set of four CMIP6 models are selected here to conduct an investigation of the errors in modern climate models in simulating CREs over CA. The CMIP6 historical simulations are from 1850 to 2014 and account for instance for radiative forcing from atmospheric composition changes due to human activities, land-use changes, and solar variability. We use the monthly mean output from March 2000–December 2014 of four historical experiments of coupled-models of CMIP6, listed in Table 1. The output variables under consideration for this study are the longwave and shortwave radiative fluxes at the TOA and at the surface for both all-sky and clear-sky conditions and the total cloud fraction (see details in Table 2). In this study, we chose the CMIP models for which the monthly output of the variables listed in Table 2 are available.

2.1.3. ERA5 reanalysis

We compute anomalies in the sea-surface temperature (SST) from the Fifth Generation Reanalysis (ERA5) produced by ECMWF. ERA5 has been widely used in various studies (Xie et al., 2019; Xia et al., 2021a, 2021b; Dommo et al., 2022; Camberlin et al., 2023; Zhang et al., 2023). ERA5 simulates the global atmosphere, land surface and ocean waves from 1950 to the present. ERA5 provides hourly data with 0.25°x0.25° horizontal resolution for a large number of atmospheric and oceanic variables and provides uncertainty information (Hersbach et al., 2020). ERA5 has benefited from a decade of development in model physics and data assimilation methods and are now based on Ensemble Data Assimilation and integrated operational forecasting system (IFS). ERA5 data does not only have a higher spatial resolution, but also many changes and improvements were incorporated into the IFS, compared to earlier global reanalysis of ECMWF. We use monthly SST for the period March 2000–December 2014 to assess the connection of the seasonal cycle in CRE to SST variability.

Table 1
CMIP6 AMIP Models used in this study.

Models	Institute/country	Horizontal resolution (lon x lat)	Vertical level
MIROC6	JAMSTEC/ Japan	1.4°x1.4°	L81
MPI-ESM1–2-LR	MPI-N/ Germany	1.875°x1.85°	L48
IPSL-CM6A-LR	IPSL/ France	2.5°x1.2°	L79
UKESM1–0-LL	Met Office Hadley Centre/UK	1.875°x1.25°	L86

Table 2
list of variables and their definition in CMIP6 AMIP Models used in this study.

Variables	Definitions	Unit
rsdt	top of atmosphere incoming shortwave flux	W/m^2
rsut	top of atmosphere outgoing shortwave flux	W/m^2
rsutcs	top of atmosphere outgoing shortwave flux assuming clear sky	W/m^2
rlut	top of atmosphere outgoing longwave flux	W/m^2
rlutcs	top of atmosphere outgoing longwave flux assuming clear sky	W/m^2
rlds	surface downwelling longwave flux in air	W/m^2
rldscs	surface downwelling longwave flux in clear sky	W/m^2
rlus	surface upwelling longwave flux	W/m^2
rlucs	upwelling longwave flux assuming clear sky	W/m^2
rsds	surface downwelling shortwave flux in air	W/m^2
rsdscs	surface downwelling shortwave flux in clear sky	W/m^2
rsus	surface upwelling shortwave flux in air	W/m^2
rsuscs	surface upwelling shortwave flux in air assuming clear sky	W/m^2
clt	Total cloud area fraction	%

2.2. Methods

In this study we calculate and analyze the CREs over the year in the region of CA bounded by 12°E-30°E & 4°S-4°N. We calculate the CREs in shortwave and longwave radiative fluxes as follows (e.g., Hill et al., 2018; Rossow and Zhang, 1995):

$$CRE = \left(F^{allsky}\downarrow - F^{allsky}\uparrow\right) - \left(F^{clearsky}\downarrow - F^{clearsky}\uparrow\right) \quad (1)$$

In this equation, $F^{allsky}\downarrow$ and $F^{allsky}\uparrow$ denote the downward and upward radiative fluxes in all sky, whereas $F^{clearsky}\downarrow$ and $F^{clearsky}\uparrow$ are the downward and upward radiative fluxes in clear sky (i.e., without clouds). We calculate both CRE at TOA and at the surface in SW and LW (SWCRE and LWCRE). Positive (negative) values of CRE at the top of the atmosphere imply a surplus (deficit) of radiation in the climate system associated with clouds. The net CRE is then obtained as the sum of the SWCRE and LWCRE (NETCRE). The in-atmosphere CRE is computed by subtracting the surface CREs from the TOA CREs. Note that at the TOA, the SW downward radiation entering the climate system in clear or in all-sky is the incoming solar radiation. Likewise, the LW downward radiation entering the climate system at the TOA in clear or in all-sky is zero.

3. Mean spatial pattern and annual cycle of CREs

3.1. Mean spatial pattern

Fig. 1 shows the long term mean spatial distribution of shortwave, longwave and net CREs for 2000–2014 from CERES satellite observations. The magnitude of the CREs vary across the area, with marked differences in CREs primarily over the Congo basin and Western Equatorial Africa encompassing Gabon, Congo republic and Equatorial Guinea.

At the top of the atmosphere, the SWCRE is negative. Conversely, the LWCRE at the top of the atmosphere is positive. This implies that the effect of clouds is to reduce (increase) the shortwave (longwave) radiation over CA. In terms of the NETCRE at the top of the atmosphere, the SW cooling of clouds dominates their LW warming leading to net cooling effects of clouds with standard deviation of about 1.9 W/m^2. Thus, clouds act to reduce energy at the TOA over CA. These results are similar

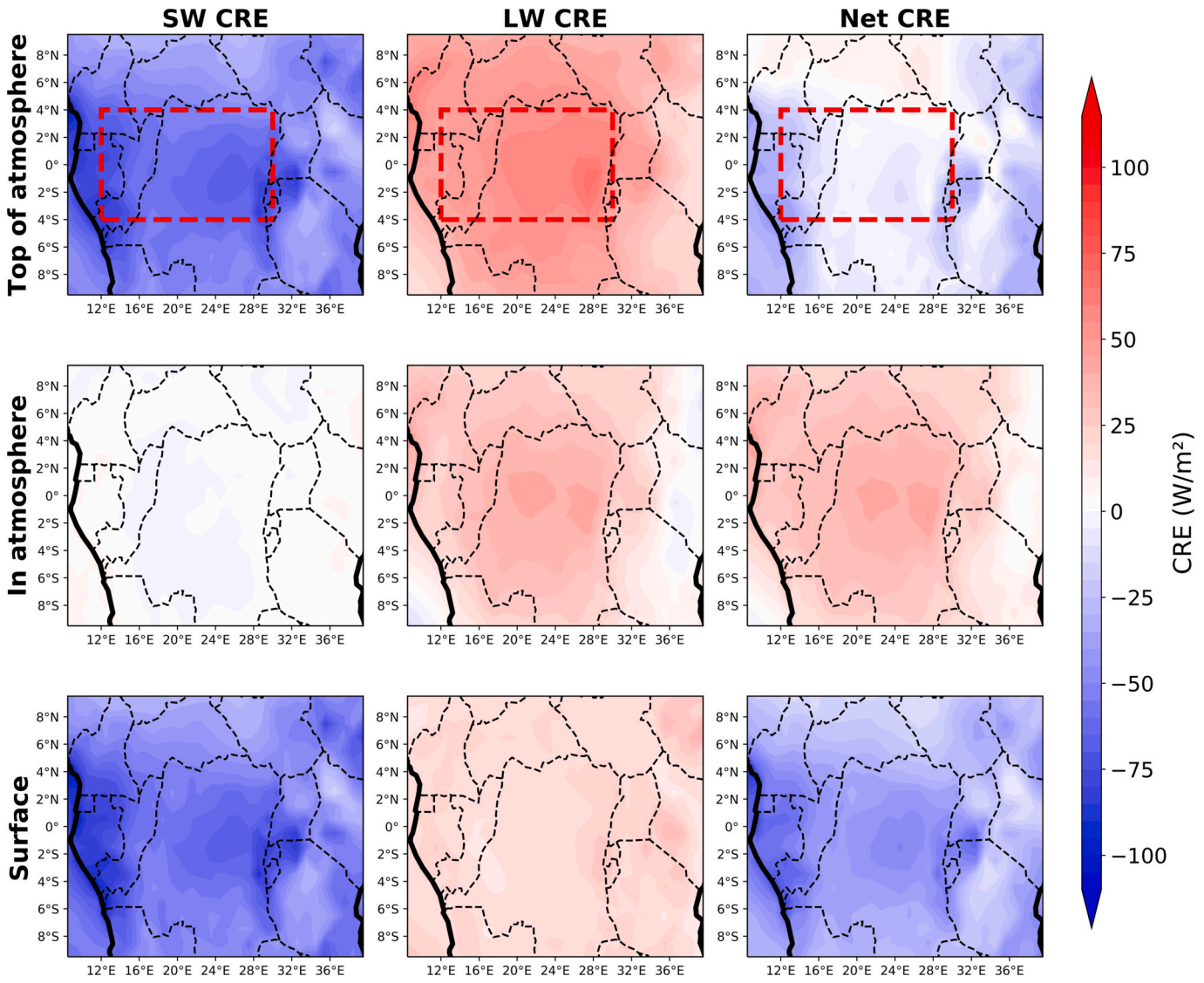

Fig. 1. Mean spatial pattern of cloud radiative effects at the top of the atmosphere (first row), in the atmosphere (second row) and at the surface (third row) for March 2000–December 2014. The first to third column are the shortwave, longwave and net cloud radiative effect. The red box delineates the boundaries of 12°E-30°E & 4°S-4°N for the area of the Congo rainforest for further analyses. These results are based on the CERES-EBAF dataset Ed4.1 level 3b. (For interpretation of the references to colour in this figure legend, the reader is referred to the web version of this article.)

to previous findings for other regions, namely Southern West Africa (Hill et al., 2018), southeastern China (Li et al., 2020a, 2020b) and the Tibetan Plateau (Li et al., 2021, 2022).

The in-atmosphere shortwave CRE is close to zero, but clouds strongly absorb longwave radiation in the atmospheric column. This enhanced absorption of the longwave radiation by clouds leads to a net gain of energy in the atmospheric column with very weak interannual variability (standard deviation =1.5 W/m^2). At the surface, the SWCRE is negative, meaning a reduction of SW radiation by clouds and thus a cooling effect of clouds at the surface. Conversely, the LW CRE is positive, indicating an increase of longwave radiation at the surface associated with clouds. As at the TOA and consistent to Hill et al. (2018) over Southern Western Africa, the shortwave cooling dominates the longwave warming leading to a net cooling (standard deviation is about 1.7 W/m^2) and an energy deficit at the surface due to clouds. Hence, the CRE over CA acts to stabilize the lower atmosphere in the climatological mean via radiative cooling at the surface and heating in the atmosphere.

3.2. Mean annual cycle

The mean seasonal variability of CRE is shown in Fig. 2 for the Congo rainforest (Fig. 2a-c) delineated by the red box on Fig. 1 and for the entire tropics (Fig. 2d-f) delineated by 180°W-180°E & 4°S-4°N. Over Congo rainforest, the bimodal cycle with two maxima observed in April and October characterize the annual cycles of many CREs in CA for all levels (Fig. 2a-c).

At the TOA, the LWCRE and the SWCRE have almost the same magnitude from January to May but with opposite signs (Fig. 2a). This leads to the compensation of the LW warming by SW cooling over CA. From June to December, shortwave cooling dominates the longwave warming leading to a slight net cooling by clouds over CA (Fig. 2a). This is interesting in comparison to the net CRE for the entire tropics (Fig. 2d), where the SW cooling dominates the LW warming throughout the year. Averaged across the tropics, clouds therefore act to cool the regional climate in the mean seasonal cyclone, but this is only true to the second half of the year over CA.

The seasonal cycle in the TOA net CRE over CA (Fig. 2a) can be linked to different radiative effects of high-altitude clouds (e.g., cirrus/

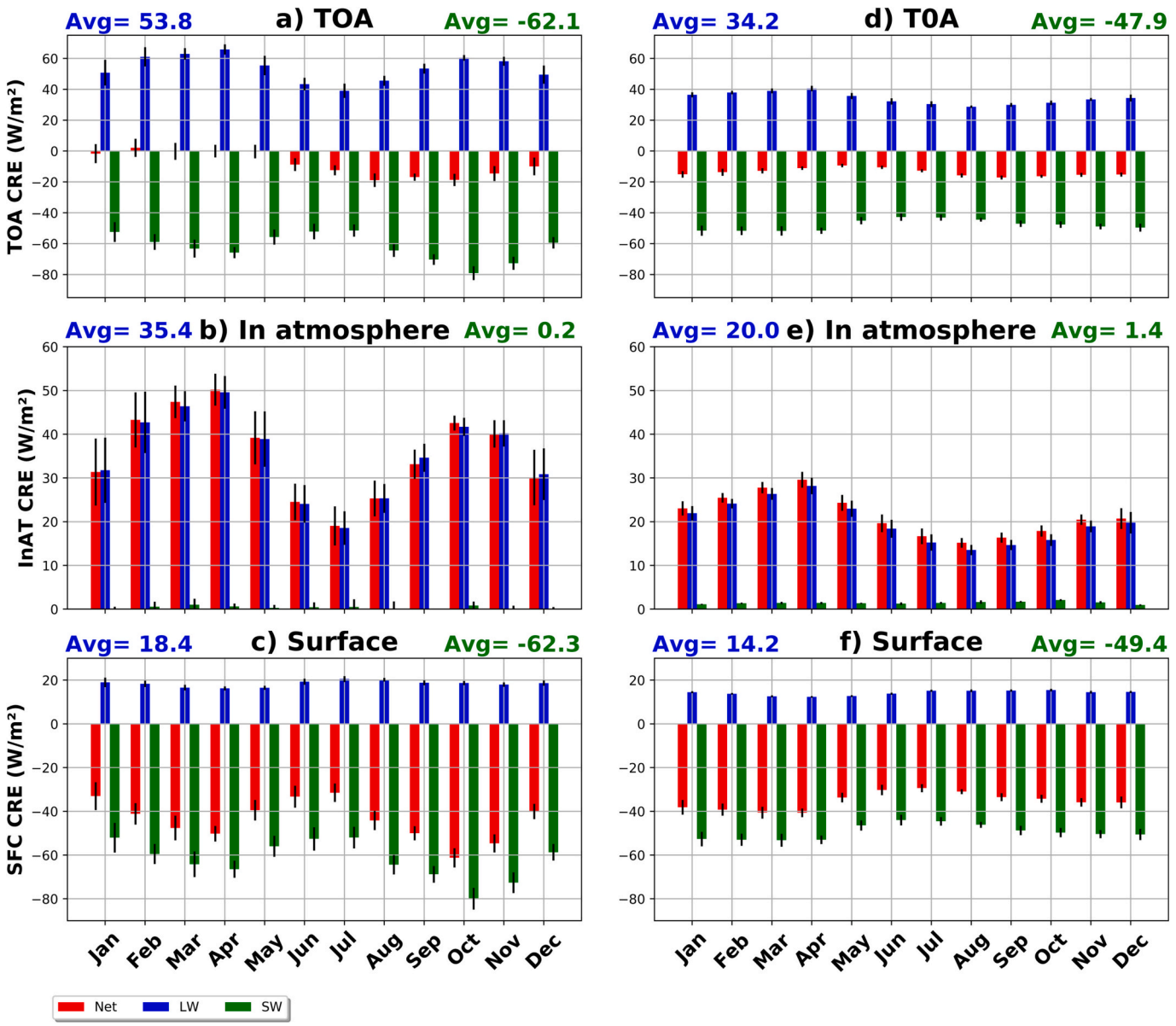

Fig. 2. Monthly means of shortwave, longwave and net cloud radiative effects at the top of the atmosphere, in the atmosphere, and at the surface over (a-c) Central Africa and over (d-f) the entire tropic using CERES data over the period March 2000–December 2014. For spatial average, we considered the boundary area 12°E-30°E & 4°S-4°N marked in Fig. 1 and 180°W-180°E & 4°S-4°N for Central Africa and the entire tropic, respectively. The blue and green values at the top of each panel are the annual mean values for longwave and shortwave clouds radiative effects, respectively. The error bars indicate the standard deviation. (For interpretation of the references to colour in this figure legend, the reader is referred to the web version of this article.)

cirrocumulus) and low clouds (e.g., Stratus/Stratocumulus). Indeed, from January to May, the enhancement of the LWCRE is associated with the development of high-altitude thin clouds (Fig. 3a) and the anomalously warm SST (Fig. 3b) over the western Atlantic coast. This result is consistent with the finding of Allan (2011) who showed that in the moist tropics, much of the LW heating of the atmosphere is especially due to high clouds. The enhancement of the LWCRE leads to the net cancellation with its SW counterparts. From June–September, anomalously cool SST (Fig. 3b) in the western Atlantic coast favors the development of low stratus clouds (Fig. 3a) which extend up to 15°E (Dommo et al., 2018, 2022), and is associated with smaller downwelling SW radiation at the surface, and then the reduction of the SWCRE at the surface. During the second half of the year, high-altitude clouds are associated with both the stronger downwelling LW warming and the stronger SW cooling compared to the global and tropical mean (Table 3), but the SW cooling dominates the LW warming leading to a net cooling effect at both the surface and the TOA compared to the first half of the year (Fig. 2a). This behavior of the TOA net CRE over CA is very different compared to the mean for the entire tropics (Fig. 2d) that is negative throughout the year due to SW cooling dominating the LW warming of clouds.

In the annual mean, the enhanced shortwave radiative reduction of -62.1 W/m^2 dominates over the longwave energy gain of 53.8 W/m^2 over CA, which implies an overall energy loss of -3.8 W/m^2 (NETCRE) at the TOA. This value (-3.8 W/m^2) is weak compared to the global and tropical averages (Table 3). This result indicates that CA gains more energy than in the global mean and more strikingly than in the mean for the entire tropics delineated by 180°W-180°E & 4°S-4°N.

At low latitudes, the cloud LW forcing is primarily within the atmosphere (Slingo and Slingo, 1988). This is also true for CA, where the mean in-atmosphere LWCRE dominates the SWCRE. Fig. 2b shows some absorption of SW radiation, but this absorption is small with an annual mean of 0.2 W/m^2. This slight heating effect relates to absorption of SW

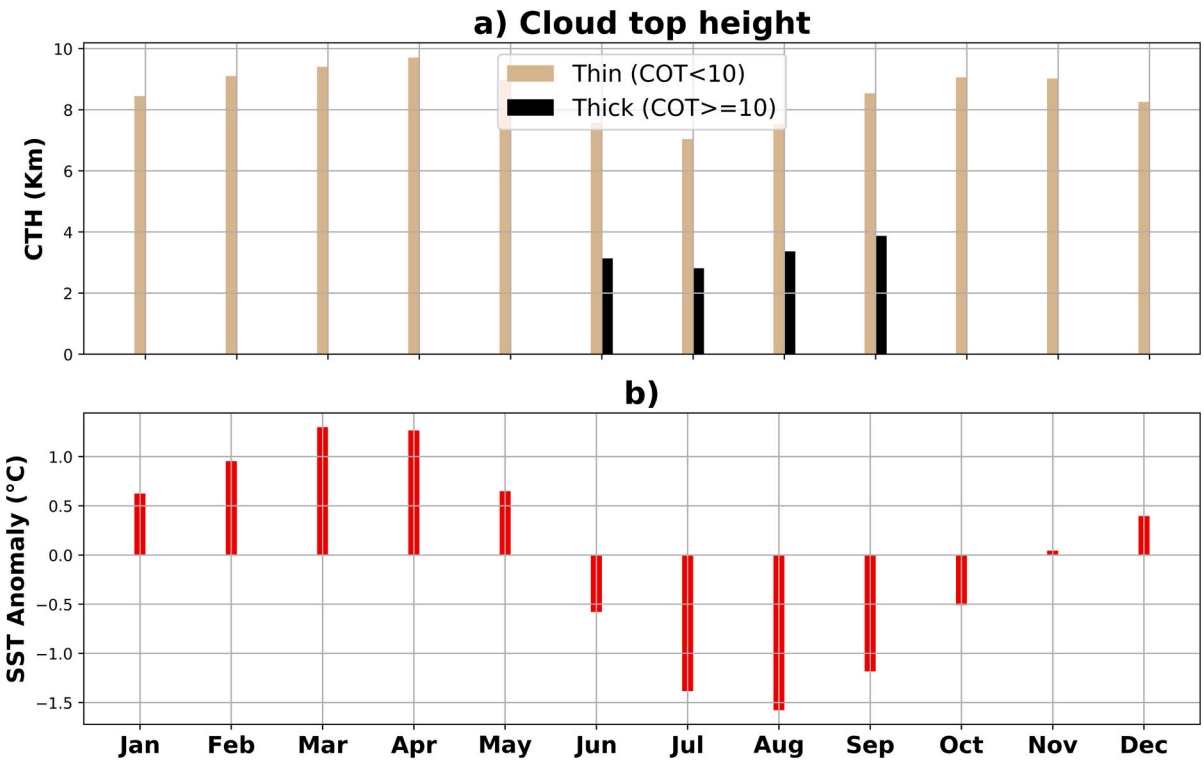

Fig. 3. Monthly variation of (a) the cloud top height for thin and thick clouds over Central Africa according to Hartman et al., (1992), (b) the standardized sea surface temperature anomaly over the West Atlantic coast from ERA5 for the period March 2000–December 2014. The west Atlantic coast is bounded by 0-8E & 4°S-4°N.

radiation by the cloudy atmosphere rather than a direct absorption of SW radiation by the cloud itself (Allan, 2011). Over most of the moist tropical area, much of the LWCRE is manifested as a heating of the atmosphere (Prata, 1996), especially in the presence of high-altitude clouds. This is also true over CA with a LWCRE of about 35.4 W/m^2. This leads to a net CRE of about 35.6 W/m^2 indicating that the atmosphere is warming over CA. Anomalously warm SST observed from January to May favors the presence of high-altitude clouds which tend to warm the atmosphere by more downwelling thermal radiation. From June to December, the development of shallow clouds over the Atlantic coast owing to anomalously cool SST (Fig. 3b) reduce the magnitude of LWCRE (Fig. 2b, e), mainly from June to August (Fig. 2b) when low stratus clouds extend from sea up to 15°E over land (Dommo et al., 2018, 2022) with the lowest LWCRE. The increasing LWCRE from July to October is associated to the increasing amount and expansion of high-altitude clouds over the study area (not shown). Indeed, the LW radiation dominates the radiative effects of clouds (Fig. 2b, e), exhibiting atmospheric cloud radiative warming above 36 W/m^2, similar to findings over the Tibetan Plateau (Wang et al., 2021). Over the whole tropical area (Fig. 2e), the absorption of shortwave radiation is slightly larger than for CA, but still relatively small with an annual mean of about 1.4 W/m^2. However, the annual mean LWCRE is larger over CA compared to the tropical and global mean estimates (Table 3) leading also to a net CRE over CA that is larger than what is observed for the tropics and the globe. Indeed, the atmospheric net CRE is positive inside the Inter Tropical Convergence Zone and associated with anomalously warm SSTs (Fig. 3b) over the tropics, consistent with previous studies using CERES-EBAF (Allan, 2011; Lin and Yu, 2022). It is noteworthy that the seasonal cycle of the SST anomaly (not shown) over the tropics shows positive values from January to June, and negative values from July to December. The anomalously cool SST from July to December would have led to negative atmospheric CRE (Lin and Yu, 2022). This suggests that even for anomalously cool SST over the tropics, thus for typically shallower clouds, there is stronger trapping of upwelling radiation from escaping the space at the TOA than at the surface, leading to a positive in- atmosphere CRE (Fig. 2b).

At the surface, the magnitude of LWCRE hardly changes over the year, with an annual mean value of 18.4 W/m^2 over CA (Fig. 2c) and 14.2 W/m^2 over the whole tropics (Fig. 2f). These values are smaller than the global mean (Table 3). In the moist tropical areas, cloud emission to the surface is small and most of the downward LW radiation originates from emission of the moisture near the surface which acts like the greenhouse layer (Prata, 1996). SWCRE is strongly negative (Fig. 2c). Over CA, as at the TOA (Fig. 2a), the variability of the SWCRE at the surface (Fig. 2c) shows two maxima: the first in March–April and the second in September–October owing to the prevalence of deep convective clouds (associated to the convective activity that leads the rainfall over CA), reflecting back more SW radiation to space. In June to August, anomalously cool SST over the western atlantic coast (Fig. 3b), partly offset the convection and favor the development of shallower thin clouds which are more transparent to SW radiation, reducing the SW cooling at the surface. This variability is also observed over the entire tropics (Fig. 2f). The SWCRE over CA acts to cool the surface with the annual mean value of −62.3 W/m^2. This value is more negative compared to the global and tropical mean (Table 3). Because the shortwave cooling dominates the longwave warming throughout the year, the net effect of clouds at the surface is cooling with an annual mean of −43.9 W/m^2. Again, this value is larger compared to global and tropical mean estimates (Table 3). In general, by reducing the outgoing thermal radiation to space, clouds in CA act to warm the surface. At the same time, clouds can reduce the warming at the surface through their high albedo by reflecting incoming shortwave radiation back to space. This ability of clouds to simultaneously cool and warm the surface depends on their optical properties that we assess in the following section.

As a summary of the contribution of clouds to annual mean energy budget, Fig. 4 shows how the net effect on atmospheric heating can be explained by contrasting SW and LW radiation effects at the surface and at the TOA. Over CA (Fig. 4a), the annual mean of net CRE is about 8.4

Table 3
Global, tropical and Central Africa annual mean estimates of the magnitude of longwave, shortwave and net clouds radiative effects. ([a]) are reference estimates from Wild et al., 2014, 2018; and ([b]) are reference estimates from **Kato et al., (2018)**. ([T]) are estimated values over the tropical boundary by 180 W-180E & 4°S-4°N for the period March 2000–December 2014. The annual mean estimates of LWCRE, SWCRE and net CRE at the TOA, in atmosphere and at the surface for each of the four models used are also indicated. The bold values are annual mean estimated in this study using CERES-EBAF Ed4.1. The mean bias between models and CERES-EBAF observations over CA are in brackets.

Energy balance component	Reference estimates at global scale	Estimates energy balance over CA and the entire tropic	MIROC6	MPI-ESM1–2-LR	IPSL-CM6A-LR	UKESM1-O-LL
		Top of the atmosphere				
LW CRE	**25.8**, 28[a]	**53.8**, **34.2**[T]	51.4 (−2.4), 38.8[T]	40.1 (−13.7), 26.4[T]	40.3 (−13.5), 29.9[T]	31.5 (−23.3), 27.4[T]
SW CRE	**−45.3**, −47[a]	**−62.2**, **−47.9**[T]	−93.1 (−30.9), −78.9[T]	−53.0 (9.2), −43.1[T]	−65.3 (−3.1), −53.3[T]	−37.9 (24.3), −45.5[T]
Net CRE	**−19.4**, −19[a]	**−8.4**, **−13.7**[T]	−41.7 (−33.3), −40.1[T]	−12.1 (−3.7), −16.7[T]	−25 (−16.6), −23.4[T]	−6.4 (2), -18.1[T]
		Atmosphere				
LW CRE	**−1.7**, 0[a], −3[b]	**35.4**, **20**[T]	24.8 (−10.6), 19.8[T]	22.8 (−12.6), 15.7[T]	23.7 (−11.7), 16[T]	25.7 (−9.7), 18.0[T]
SW CRE	**3**, 7[a], 4[b]	**0.2**, **1.4**[T]	3 (2.8), 2.1[T]	0.9 (0.7), 1.7[T]	6.0 (5.8), 4.8[T]	−1.0 (−1.8), 0.8[T]
Net CRE	**1.3**, 7[a], 1[b]	**35.6**, **21.4**[T]	27.8 (−7.6), 21.9[T]	23.7 (−11.9), 17.4[T]	29.7 (−5.7), 20.8[T]	24.7 (−10.9), 18.8[T]
		Surface				
LW CRE	**27.5**, 28[a], 30[b]	**18.4**, **14.2**[T]	26.6 (8.2), 19.1[T]	17.4 (−1), 10.7[T]	16.6 (−1.8), 13.9[T]	5.8 (−12.6), 9.4[T]
SW CRE	**−48.3**, −54[a], −50[b]	**−62.3**, **−49.3**[T]	−96.1 (−38.8),− 81.01[T]	−54 (8.3),− 44.8[T]	−71.4 (−9.1),− 58.1[T]	−36.8 (25.5), −46.3[T]
Net CRE	**-20.7**; -26[a], −20[b]	**−43.9**, **−35.1**[T]	−69.6 (−25.7), −61.9[T]	−36.6 (7.3), -34.1[T]	−54.7 (−10.8), -44.2[T]	−31 (12.9), −36.9[T]

Fig. 4. Schematic illustrating the annual mean values estimated of CRE components (LW, SW and NET) over (a) Central Africa, (b) global and (c) entire deep tropics at the TOA, in the atmosphere and at the surface from CERES-EBAF Ed4.1 for the period March 2000–December 2014. In this study, Central Africa is bounded 12°E-30°E & 4°S-4°N whereas the entire deep tropics is bounded 180°W-180°E & 4°S-4°N. The direction of each arrow indicates the direction of CRE in its corresponding component and the size of each arrow is proportional to the magnitude of CRE. Down (Up) oriented arrows signify cloud radiative warming (cooling) effect.

W/m^2 which is less compared to global (Fig. 4b) and tropical (Fig. 4c) mean values estimated. The net heating in the atmosphere over CA (Fig. 4a) and over the entire tropic (Fig. 4c) is the combination of both the SW and LW clouds heating effect, while over the global scale (Fig. 4b), the SW heating is attenuated by the LW cooling effect of clouds. Clouds have the same effect on radiative components at the TOA and at the surface over CA as over global or tropical scale. Indeed, whether over CA, over the entire tropic or at the global scale (except for Artic and Antartic regions), there is always a LW (SW) warming (cooling) at the TOA and at the surface with SW cooling dominating the LW

warming. This domination of CRE by SWCRE is consistent with the findings over Eastern China (Li et al., 2017). Overall, the LWCRE and SWCRE over CA (Fig. 4a) are larger compared to global (Fig. 4b) and tropical (Fig. 4c) scales.

4. Relationships between cloud optical properties and CREs over CA

The dependence of the CRE on cloud characteristics has been inferred in many studies (Hartmann et al., 1992; Rossow and Zhang, 1995), but none addressed it for CA. For instance, deep clouds are more effective in altering the TOA longwave radiation because they are relatively colder than the surface and the lower atmosphere, whereas low-level clouds have little effect longwave radiation at the surface because they have a similar temperature like their environment. Cloud types have different effects on the shortwave radiation transfer. For instance, high thin clouds are nearly transparent to solar radiation but partially absorb longwave radiation.

We explore to what extent the relative importance of the shortwave and longwave effects of clouds can be explained by cloud properties. Factors affecting CRE include for instance the cloud optical thickness (COT), cloud-top height (CTH), area of cloud coverage (Ramanathan et al., 1989; Jiang et al., 2022) and cloud top temperature (CTT) (Lin and Yu, 2022). Here, we investigate the relationships between the LWCRE, SWCRE, and NETCRE against such cloud properties. To quantitatively assess the link between monthly CRE and cloud optical properties, we calculated the Pearson correlation coefficients and performed a two-sided *t*-test with a 95% level for significance.

4.1. Spatial pattern

We first assess the spatial patterns of cloud properties that allows us to spatially link the cloud properties to CRE components. Fig. 5 shows the geographical distribution of the mean total cloud fraction (TCF) (Fig. 5a), CTH (Fig. 5b), COT (Fig. 5c) and CTT (Fig. 5d). The highest cloud fraction (Fig. 5a) of about 80% prevails over the Central Congo basin and the Western Central Africa (WCA) encompassing Gabon, Congo, Equatorial Guinea and the coastal part of south Cameroon. Likewise, as for the TCF, the CTH is the highest (>8 km) and conversely, the CTT is the coldest (< 250 K) over the CA, with mean COT<23. These characteristics of clouds over CA exhibit the predominance of optically thin high level ice clouds (Chen et al., 2000; Burleyson et al., 2015) as their CTT < 260 K and their CTH > 8 km. In fact, Chen et al. (2000) argued that clouds with CTT < 260 °k are ice clouds and liquid otherwise. Fig. 1 and Fig. 5 show some similarities. Firstly, the peaks of SWCRE and LWCRE at the TOA and the SWCRE and NETCRE at the surface (Fig. 1) over CA coincides with the location of the peaks of TCF (Fig. 5a) and eventually the peaks of the COT (Fg 5c). Secondly, the peaks of the LWCRE and NETCRE in the atmosphere (Fig. 1) over CA correspond to the highest CTH (Fig. 5b) and the lowest CTT (Fig. 5d) and

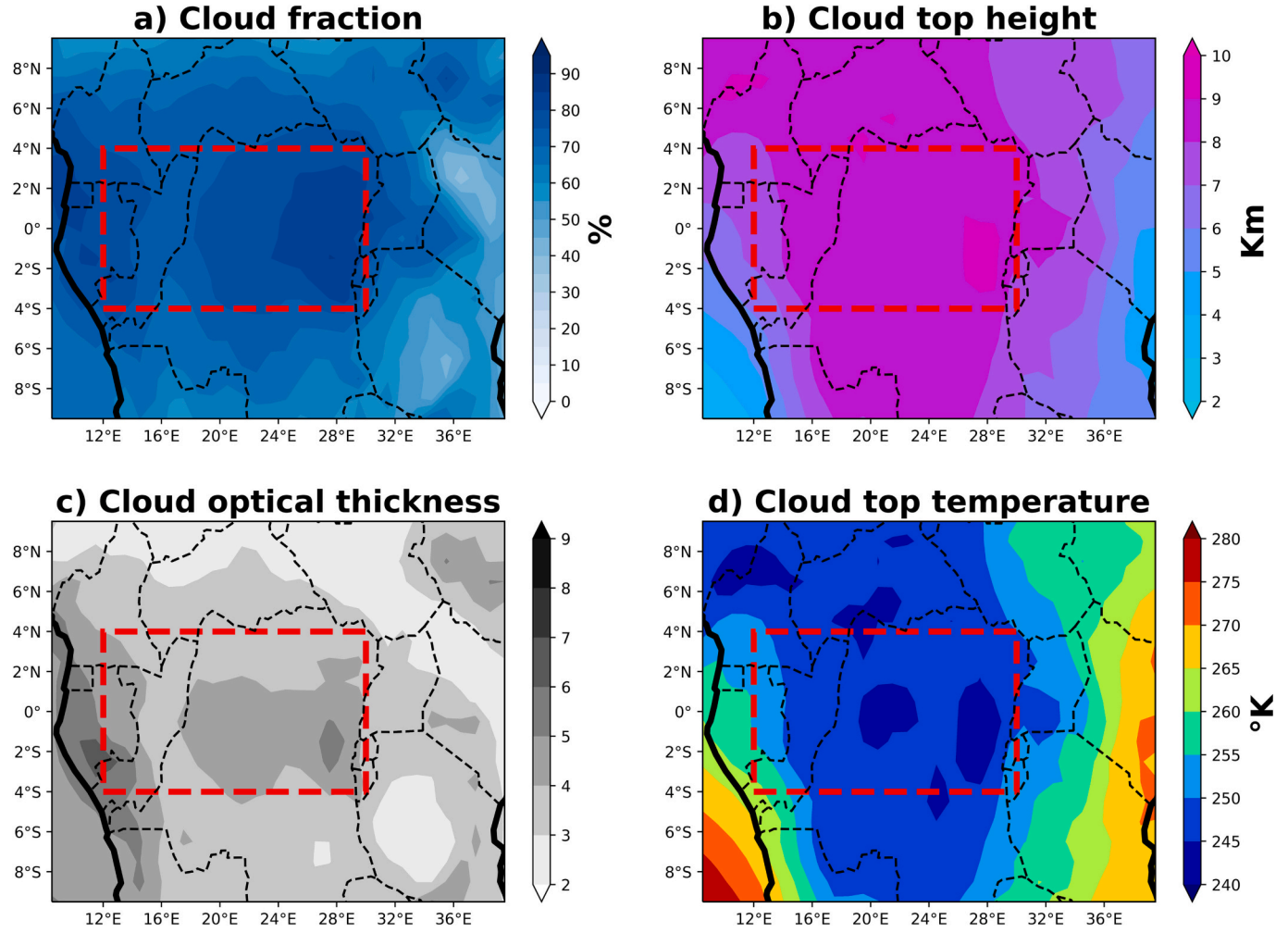

Fig. 5. Long term mean geographical distribution of a) total cloud fraction, b) cloud top temperature, c) cloud optical depth, d) cloud top temperature based on CERES-SYN1deg edition 4A (March 2000–December 2014). The red dashed box delineates the area of interest on 12°E-30°E & 4°S-4°N. (For interpretation of the references to colour in this figure legend, the reader is referred to the web version of this article.)

cloud top pressure (not shown). This finding is consistent to Lin and Yu (2022) who found that the spatial distribution of CTT is similar to that of the atmospheric net CRE with positive atmospheric CRE occurring over the area of lowest CTT (Fig. 5d). In the following, we analyze the relative dependence of the CREs to cloud properties. As for Fig. 2, we do our analysis focusing on the area bounded by 12°E-30°E & 4°S-4°N.

4.2. Total cloud fraction

Cloud fraction is one of the most important cloud parameters that influence the Earth's energy balance. The influence of cloud fraction on radiative fluxes can be inferred from previous studies (Hartmann et al., 1992; Rossow and Zhang, 1995; Jiang et al., 2022). For instance, high level clouds are most effective in altering TOA outgoing longwave fluxes because they are relatively colder than the surface. This is true over CA, where the effect of TCF (mostly the high-level clouds) on radiation is felt both on SW (Fig. 6a) and LW (Fig. 6b) radiation at the TOA. At the TOA, there is a strong temporal correlation between SW (LW) cooling (warming) (Fig. 6a, b) and TCF with correlation coefficients being −0.65 and 0.73 for SW cooling and LW warming respectively. The increase in TCF also increases both the SW cooling and the LW warming effects. This leads to a non- linear relationship and to a very weak and not significant correlation between TCF and the TOA NETCRE (Fig. 6c) due to the offsetting effect between SWCRE and LWCRE. The in-atmosphere SWCRE shows weak positive correlation with TCF (Fig. 6d) whereas its LW (Fig. 6e) counterpart exhibits strong significant positive correlation ($r = 0.65$)) with TCF. This leads to a strong positive correlation ($r = 0.70$) between the NETCRE and the TCF in the atmosphere (Fig. 6f) where the net warming effect is enhanced by the increasing TCF. At the surface, whereas the SWCRE exhibits a strong linear relationship ($r = -0.70$) with TCF with the increase of TCF leading to increasing SW cloud radiative cooling (Fig. 6g), there is no relationship with the LW warming (Fig. 6h). This leads to strong correlation with the net cloud radiation cooling (Fig. 6i). Overall, over CA, the TCF is an important contributing factor to the warming in the atmosphere as it both increases the SW and LW cloud warming effect. Likewise, adding clouds by increasing the fractional coverage area can increase shortwave cooling effect both at the TOA and at the surface, and increase the longwave warming at the

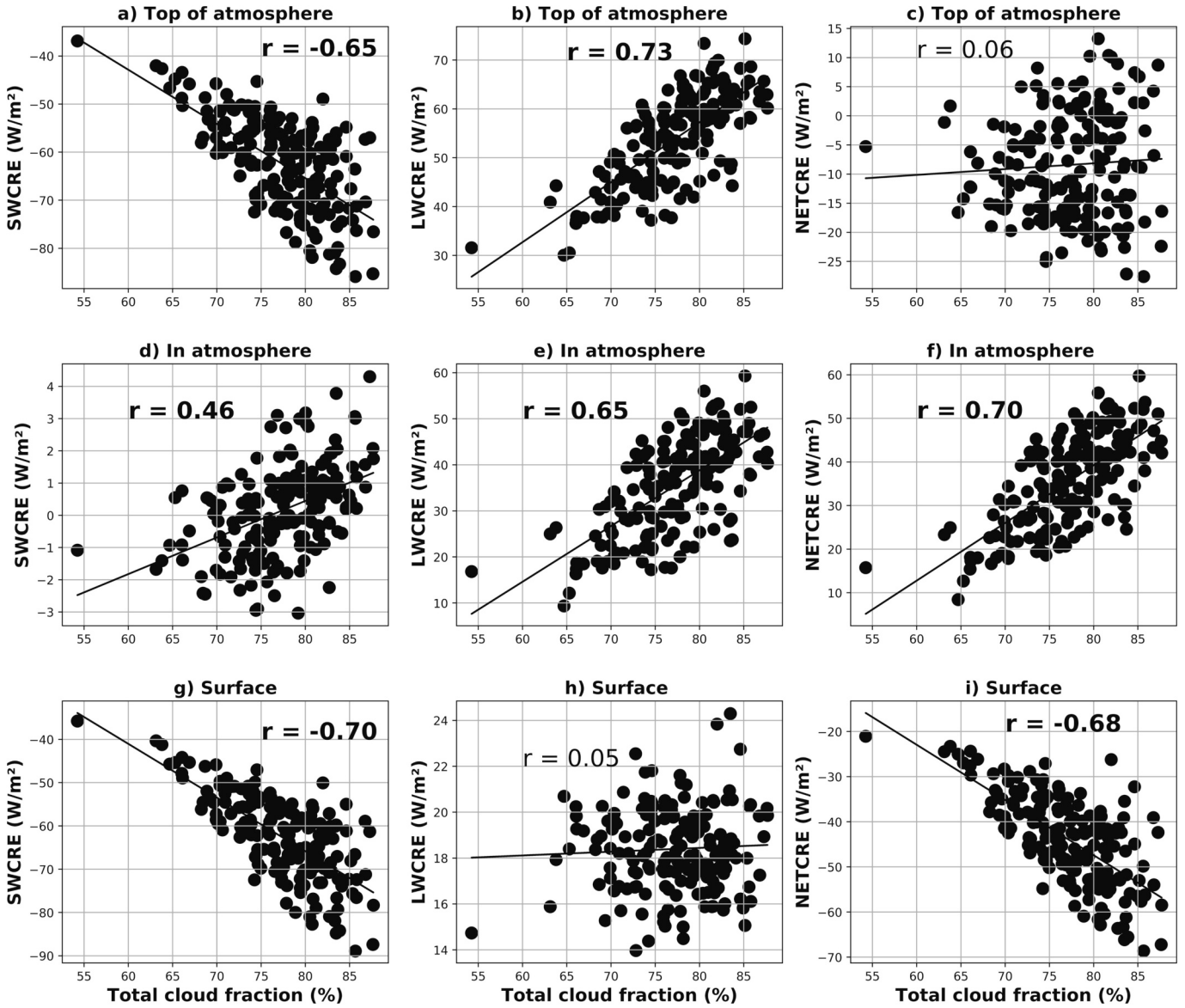

Fig. 6. Scatter plots between CREs components (SW, LW and NETCRE) and total cloud fraction at the top (first row), in atmosphere (second row) and at the surface (third row). Each black dot corresponds to the average from CERES-EBAF Ed41 of each month over the period March 2000–December 2014. The spatial average is performed over 12°E-30°E & 4°S-4°N. Significant Pearson correlation coefficients (r) at two-sided 95% level according to *t*-test are displayed in bold.

TOA.

4.3. Cloud top height

The CTH is a fundamental parameter, describing the vertical distribution of clouds, which partly determines whether clouds exert a warming or cooling effect on the planetary radiation budget. In this section we evaluate the relationship between CRE components and CTH. First of all, all the correlations between CRE components and CTH are significant over CA (Fig. 7). At the TOA, as the CTH increases, the SWCRE (Fig. 7a) and LWCRE (Fig. 7b) get large and their correlation with CTH are −0.35 and 0.83 respectively. But the true impact of CTH on net CRE is nonobvious (even though the correlation is moderate (Fig. 7c)), it turns from cooling to warming effect. Most of the clouds with CTH < 7 km (medium clouds) exhibits a net cooling effect at the TOA, whereas those with COT>7 km (high clouds) show an effect ranging from cooling to warming. Based on the CTH values, the clouds type in presence may be altocumulus, cirrostratus and cirrus (Burleyson et al., 2015; see their Table 2). As at the TOA, the effect of CTH on SWCRE and LWCRE are the same in the atmosphere (Fig. 7d,e), but it is now clear that the increasing CTH strongly increases the net cloud radiation warming with correlation being 0.83 (Fig. 7f). At the surface, the effect of CTH on SWCRE is the same as at the TOA with low correlation (Fig. 7g). Conversely to what is observed at the TOA and in the atmosphere, the increasing CTH decreases the LW cloud radiative warming (Fig. 7h) and increases the net CRE cooling effect at the surface (Fig. 7i). The correlation between the CTH and CRE component whether we are at the TOA, at the surface or in the atmosphere, shows that the CTH has the strongest effect on LWCRE. Furthermore, comparing how the correlation line between CTH and the net CRE behaves at the TOA, in the atmosphere and at the surface, it comes out that the high clouds (CTH > 7 km) strongly warm the atmospheric column and cool the surface whereas its effect at the TOA is nonobvious. In practice, the higher CTH associated with deep clouds (Casey et al., 2015) warms the atmosphere by decreasing the upwards emission of LW radiation (Slingo and Slingo, 1988).

4.4. Cloud top temperature

The CTT is one of the key cloud properties controlling the CRE (Zhao et al., 2022) with strong influence on LWCRE at the TOA. This forcing is usually positive, and largest for clouds with coldest cloud tops. In this

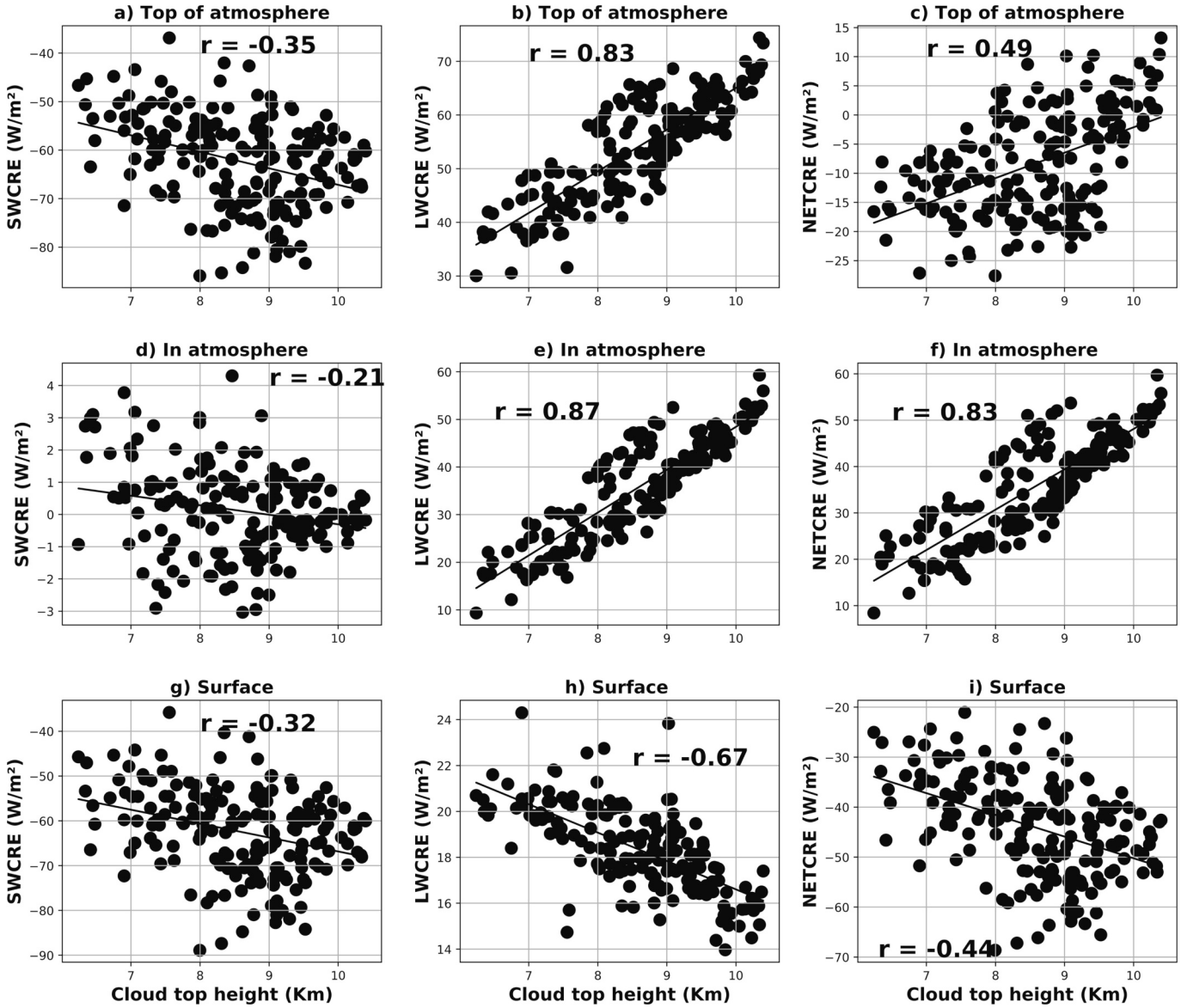

Fig. 7. As Fig. 6 but for CREs components and cloud top height.

study, the scatter plots together with the correlation coefficient between CTT and CRE components are shown in Fig. 8. We first notice that all the correlations between CTT and CRE components are significant. At the TOA, CTT shows weak positive correlation of 0.36 with SWCRE, with lower (larger) CTT corresponding to larger (lower) SW cloud radiative cooling effect (Fig. 8a). The effect of CTT on the LW cloud warming effect is very sensitive with increasing CTT leading to the decreasing LW cloud warming effect (Fig. 8b). The correlation coefficient between CTT and LWCRE is −0.83. The exact effect of CTT on net CRE is not obvious, it turns from positive net CRE for smaller CTT to negative net CRE for larger CTT (Fig. 8c). The correlation coefficient between CTT and net CRE is weak (−0.48). In the atmosphere, CTT has a slight impact on SWCRE (Fig. 8d). The correlation coefficient is weak (0.22). This may be due to the fact that the SW absorption is mostly from the atmosphere than from the clouds itself (Allan, 2011). Rather, the impact of CTT on LW and net cloud radiative warming is strong with correlation being −0.87 and − 0.82 respectively (Fig. 8e, f). The increasing CTT decreases the LW and net warming effect of clouds in the atmospheric column (the smaller the CTT, the larger the LW and net CRE and vice versa). At the surface, the relationships between CTT and CREs components are shown in Fig. 8g-i. The CTT at the surface acts to decrease the SW (Fig. 8g) and net (Fig. 8i) cloud cooling effect whereas it acts to increase the surface LW cloud warming effect (Fig. 8h). The correlation between CTT and LWCRE is moderately high (0.65) whereas the ones with SW and net CRE are low and are 0.32 and 0.44 respectively. Indeed, whether we are at the TOA, at the surface or in the atmosphere, the correlation between CTT and SWCRE are weak, whereas the correlation with the LW counterparts is strong. This result is consistent with the finding of Zhao et al., 2022 who shows that the TOA LWCRE is decided by the CTT. Likewise, our result also shows that the in-atmosphere CRE warming is strongly decided by the CTT, namely on the LW and the net CRE component.

4.5. Cloud optical thickness

Recent finding (Chen et al., 2000) shows that the largest SWCRE and LWCRE both at the TOA and at the surface are produced by clouds with the largest COT. Especially, optically thick clouds (COT≥ 10, Hartmann et al., 1992) produce a strong SW cooling effect compared to optically thin ones (COT<10). In this study, the impact of the COT is to increase the SW and NET cloud cooling effect at the TOA (Fig. 9a, c). The correlation coefficient between COT and SW (net) CRE is −0.50 (−0.62). There is no effect of COT on LWCRE at the TOA (Fig. 9b). At the TOA, the

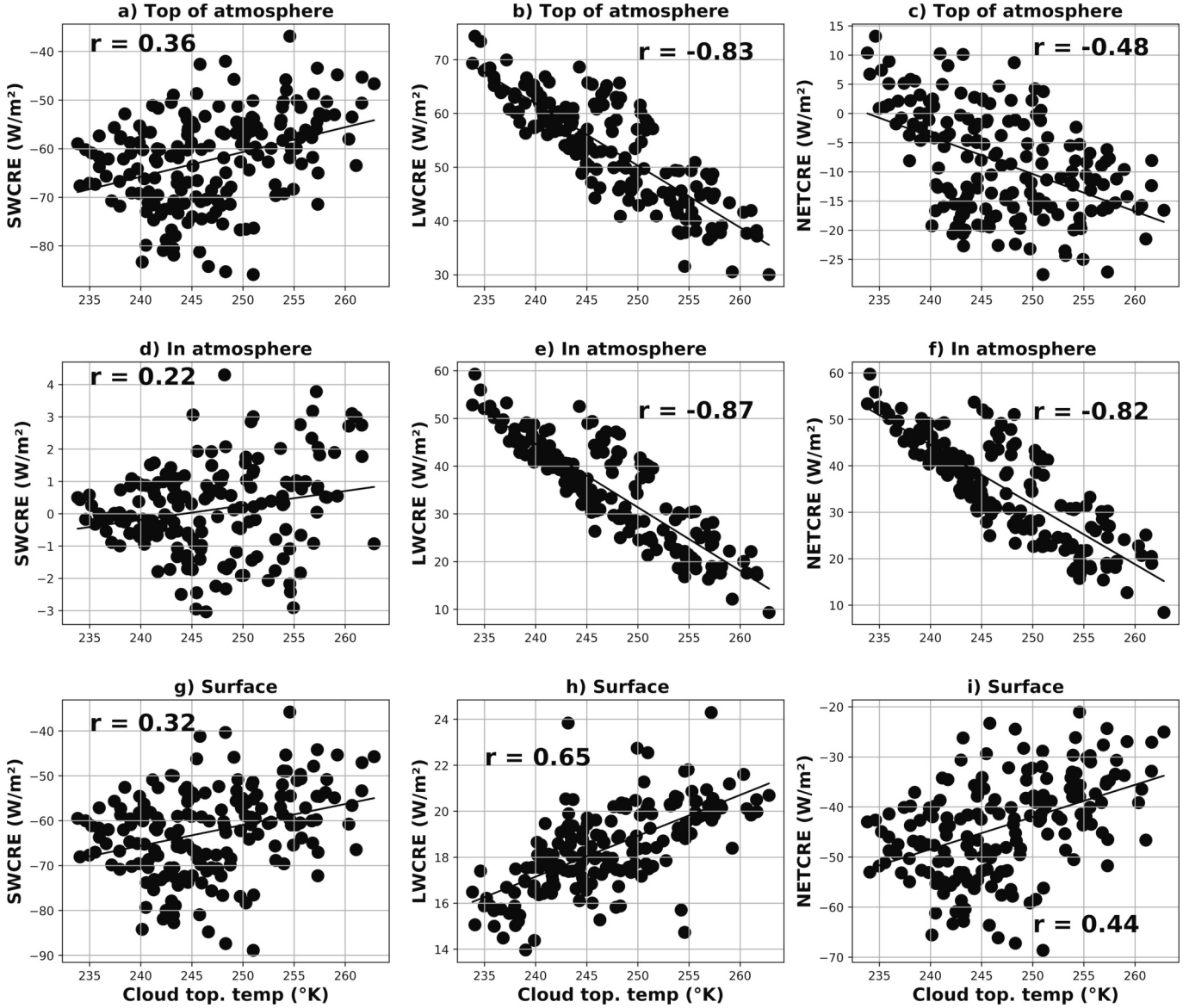

Fig. 8. As Fig. 6 but for CREs components and cloud top temperature.

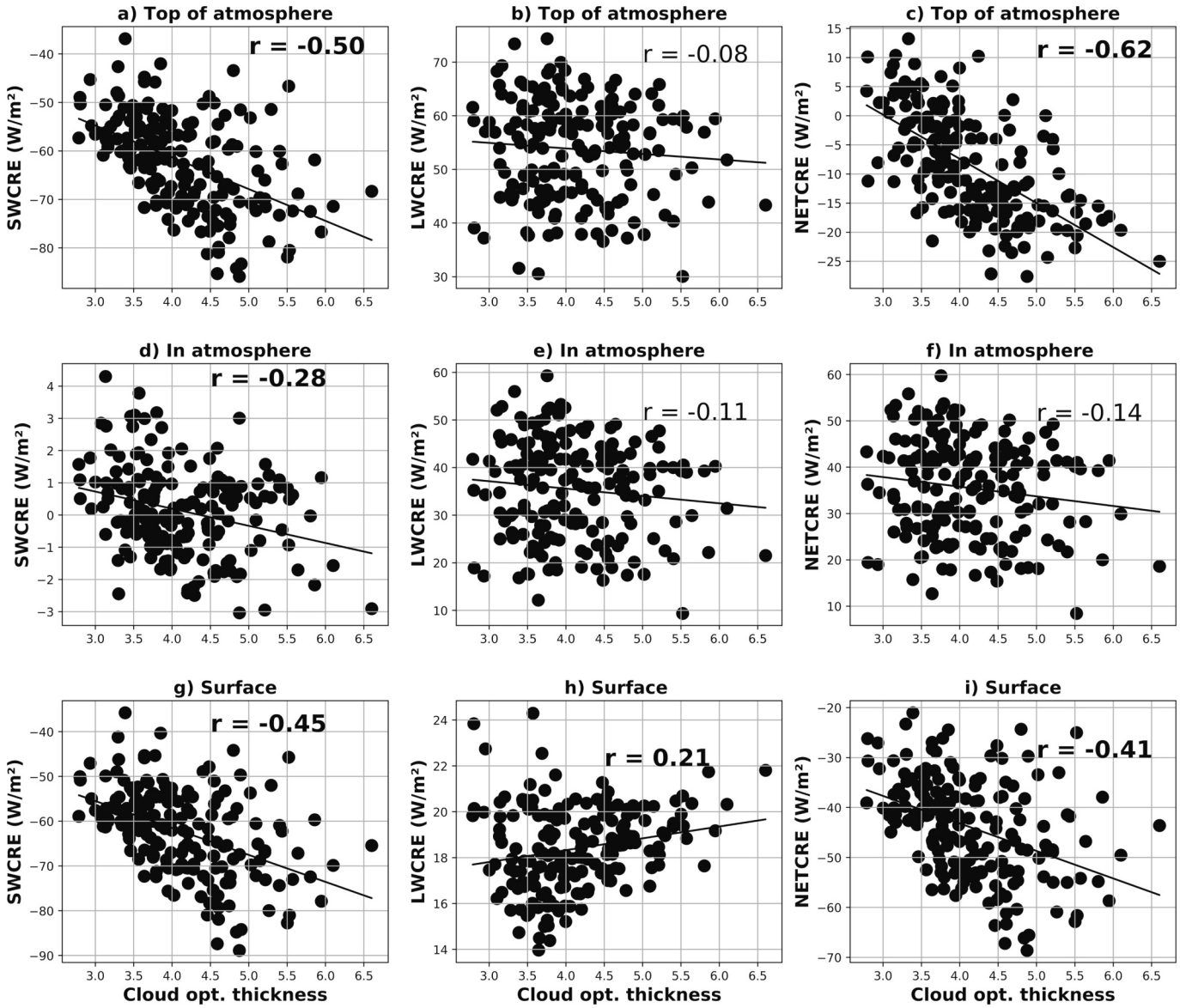

Fig. 9. As Fig. 6 but for CREs components and cloud optical thickness.

increasing COT increases the SW cloud cooling effect (Fig. 9a) with average correlation coefficient ($r = -0.5$). In the atmosphere (Fig. 9d-f), the correlations between COT and CRE components are weak. They are −0.28, −0.11 and − 0.14 for SW, LW and Net CRE respectively. At the surface, all the correlations are significant (Fig. 9g-i). As like the TCF, the impact of COT on CRE components behave the same. At the surface, the increasing COT increases the SW (Fig. 9g), the net (Fig. 9i) cloud radiative cooling and the LW cloud warming (Fig. 9h) with correlation being −0.45, −0.41 and 0.21 respectively. Overall, the SW and net cloud cooling effect increase as the COT turns from optically thin to optically thick clouds both at the TOA and at the surface, consistent with the results from Chen et al. (2000) who show that the largest magnitude of SWCRE is produced by the largest mean COT.

Overall, our results show that LWCRE is more sensitive to TCF, CTH and CTT at the TOA and in the atmosphere. At the TOA, SW cloud cooling effect is mostly sensitive to cloud fraction and optical thickness. This result is consistent with the findings from Zhao et al. (2022). At the TOA, adding more high clouds by increasing their fractional coverage area, increases the longwave warming in response to their cooler top temperature. In the atmosphere, the increasing CTT reduces or attenuates the longwave heating due to increasing TCF (Fig. 6a) and CTH (Fig. 6b) in the atmospheric column. At the surface, SWCRE is more sensitive to the TCF and COT whereas LWCRE is more sensitive to CTH and CTT with high clouds having a weak effect on LWCRE. The mean CTH ranges from 6 to 10.5Km suggesting the presence of middle to high level clouds (Chen et al., 2000). Anomalously warm SST will also promotes the development of deep convective clouds (e.g., cumulonimbus and congestus clouds), which are often accompanied by anvil clouds near the tropopause. This suggests that the CRE over CA is not due to a single cloud type. As demonstrated by Chen et al. (2000), near the equator, the largest LWCRE at the TOA and in the atmosphere is produced by cirrostratus and deep convective clouds, whereas at the surface, the largest LWCRE is produced by stratus/stratocumulus clouds. Furthermore, thicker clouds are likely to produce large SW cooling compared to their thinner counterparts. Therefore, the contribution of the different cloud types to CRE over CA will be the subject of our future work.

5. Comparison to climate models

We now undertake a preliminary assessment of CMIP6 simulations over CA, using atmosphere only simulation models that provide the set

of variables necessary to investigate the seasonal cycle of CRE at the TOA, in the atmosphere and at the surface. Here we investigate the CREs as simulated by models as well as their bias in the seasonal cycle.

5.1. Mean spatial distribution of CREs

Clouds reflect the fraction of solar radiation that would be absorbed at the Earth's surface, and they also contribute to the greenhouse effect. For the convective area, particularly the tropical areas, the two effects of clouds nearly cancel one another so that the net effect of clouds is small. This characteristic is observed over the Congo Basin for CERES-EBAF at the TOA (Fig. 1 & Fig. 10). For CERES observation, the spatial distribution of the TOA NETCRE shows a net cloud cooling effect (SW cooling dominates LW warming) along the coastal area, and in the most eastern part of the Democratic Republic of Congo whereas northern part of Cameroon and Nigeria show a slightly net warming effect (LW warming dominates SW cooling). MIROC6 and IPSL-CM6A-LR struggle to reproduce the intensity of the TOA NETCRE, as they overestimate the magnitude of the net clouds cooling effect whereas MPI-ESM1–2-LR and UKESM1–0-LL do better in simulating the TOA net clouds cooling effect. A strong cooling effect is particularly observed for MIROC6 whereas UKESM1–0-LL exhibits a slight underestimation over the WEA part. Overall, models can reproduce the spatial pattern of the SW (LW) clouds radiation cooling (warming) effect (Fig. S1).

The In atmosphere (surface) NETCRE exhibits a strong warming (cooling) effect in almost all parts of CA. This effect of clouds in the atmosphere (at the surface) is well captured by the models, but they all exhibit a slight underestimation over all parts of the CA (not shown). At the surface, MIROC6 and IPSL-CM6A-LR overestimate the intensity of the net clouds cooling effect over CA whereas MPI-ESM1–2-LR and UKESM1–0-LL do otherwise. Overall, models can capture the spatial pattern of clouds radiation effect over CA both in SW and LW

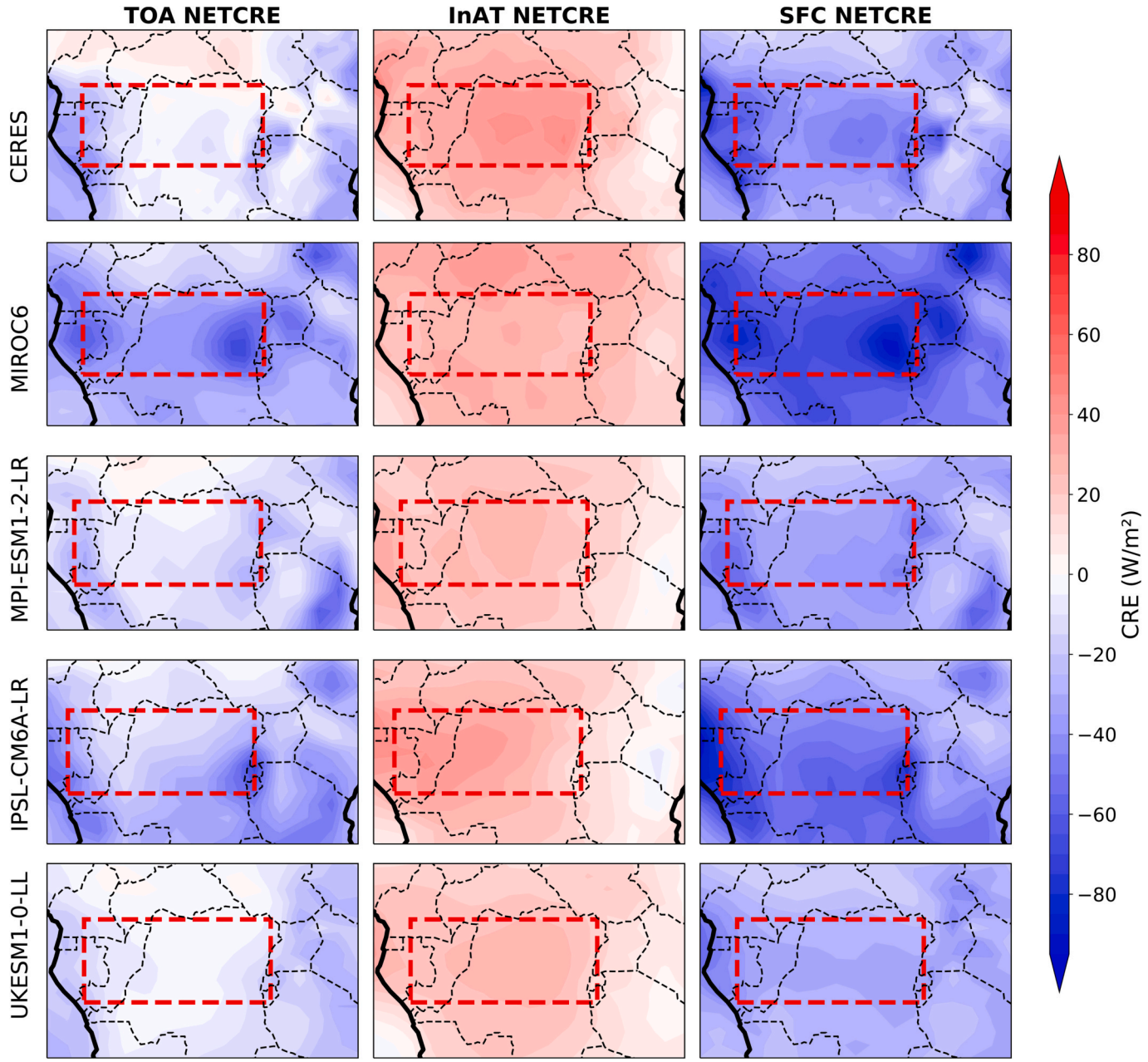

Fig. 10. Long term (March 2000–December 2014) mean spatial distribution of the net cloud radiative effect at the TOA (first column), In atmosphere (second column) and at the surface (third column) using CERES-EBAF and four CMIP6 models.

components (Fig. S2 & Fig. S3), but they struggle in simulating the intensity of the NET CRE (Fig. 10), highlighting biases in the models' simulations.

5.2. Seasonal cycle and the mean bias of CREs

At the TOA, all the models can capture the seasonal variability of SW and LW CRE (Fig. S4 b,c), but struggle to capture the seasonal variability of the NETCRE (Fig. 11a, Fig. S5d). Among the models, MIROC6 exhibits the larger amplitude of the CREs components (SW, LW, NET) along the seasonal cycle (Fig. S4b-d) with the annual mean amplitude being −93.1 W/m^2, 51.4 W/m^2 and − 41.7 W/m^2 for SW, LW and NETCRE respectively over CA. This leads to the largest annual mean bias of −30.9 W/m^2, and − 33.3 W/m^2 for SW, and NETCRE respectively (Table 3). It is worth mentioning that the mean bias is computed as the difference between the models' annual mean and the observation. It is also worth noting that because of the negative (positive) value of SW and NETCRE (LWCRE), the negative bias in NET, SW (LWCRE) components signifies an overestimation (underestimation) and vice versa. Along the seasonal cycle, UKESM1–0-LL and MPI-ESM1–2-LR underestimates the TOA SW cooling effect, whereas MIROC6 and IPSL-CM6A-LR do otherwise except in June–July-August for IPSL-CM6A-LR (Fig. S5b). All the models underestimate the TOA LW clouds radiative warming over CA along the seasonal cycle except MIROC6 which shows an overestimation in September–October-November (Fig. S5c). Again, all the models overestimate the net cloud cooling effect at the TOA along the year (Fig. S5d, Table 3) with larger mean bias, except UKESM1–0-LL which do otherwise. The latter model slightly underestimates the net CRE with an annual mean bias of 2 W/m^2 (Table 3). MIROC6 exhibits the largest annual mean bias of NETCRE in February–March-April and in September–October-November. This larger magnitude of the annual mean bias of the net cloud cooling effect at the TOA by MIROC6 is mostly due to the large magnitude of the overestimation of SW clouds radiative cooling effect (Fig. S5b, Table 3). In contrast, the slightly mean bias in NETCRE depicted by UKESM1–0-LL (Fig. 11b) is mostly due to the near cancellation of the sum of the amplitude of the bias in SW cooling and LW warming rather than the good simulation of LW and SW CRE by this model (UKESM1–0-LL). Indeed, UKESM1–0-LL underestimates both the shortwave cooling and longwave warming at the TOA with the mean bias respectively being 24.3 W/m^2 and − 23.3 W/m^2 (Fig. S5b, c, Table 3). For MIROC6 and IPSL-CM6A-LR, the mean bias in NETCRE at the TOA is mostly due to both the combination of the overestimation of the SW cooling and the underestimation of LW warming. As for UKESM1–0-LL, MPI-ESM1–2-LR underestimates both the SW cloud radiative cooling and LW clouds radiative warming.

In the atmosphere, the seasonal cycle of the SWCRE (Fig. S6b) does

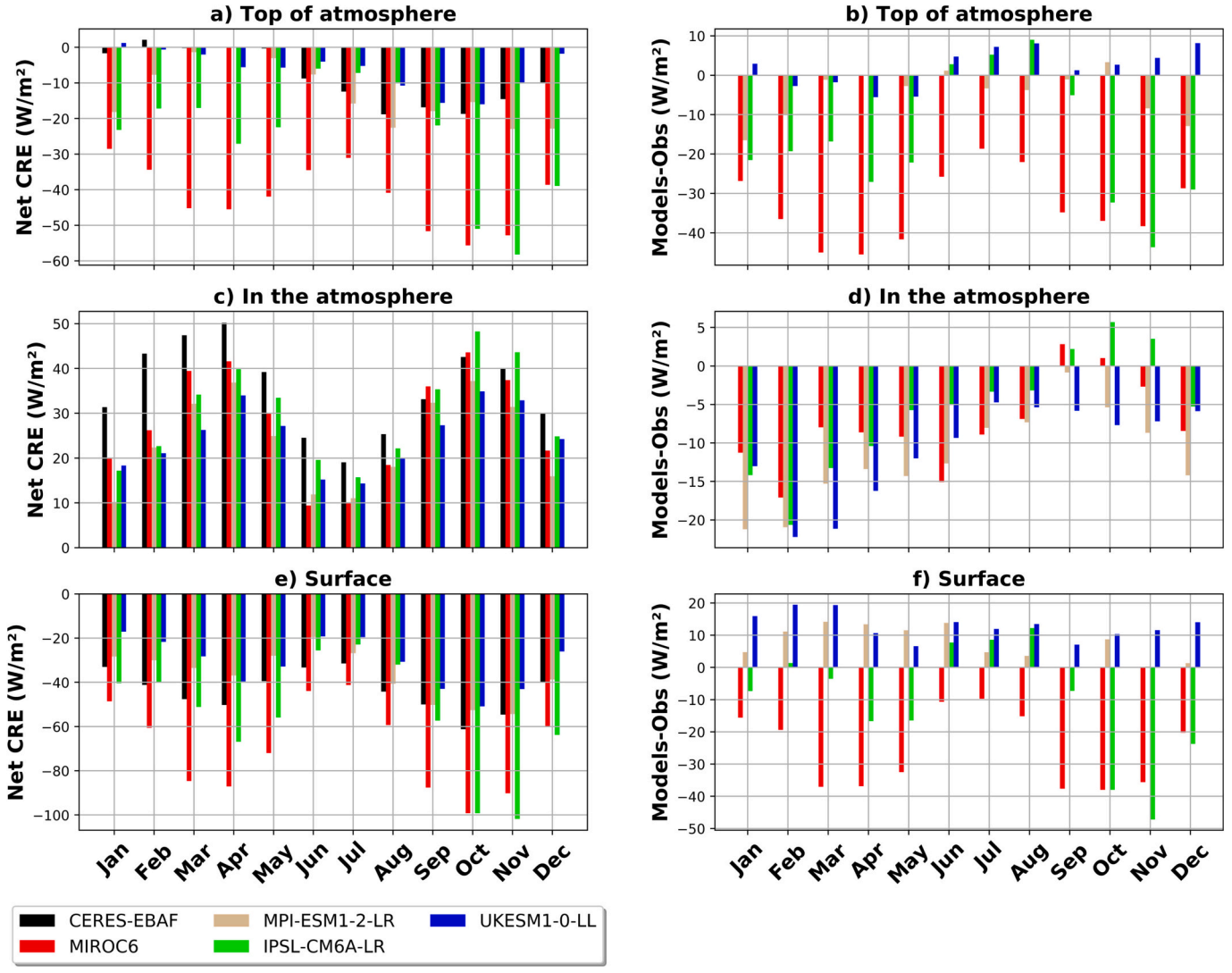

Fig. 11. Long term monthly mean bias between models and observation of net cloud radiative effect at the top of atmosphere, in the atmosphere and at the surface for the period March 2000–December 2014, averaged over 12°E-30°E & 4°S-4°N. The bias is computed as the difference between models and observation.

not have a particular shape compared to LWCRE (Fig. S6c) which exhibits a bimodal cycle well captured by all the models and with larger amplitude compared to their SW counterparts. All the models capture the bimodal cycle of the net CRE (Fig. 11c, Fig. S6d). Likewise, models exhibit a SW cloud warming effect with exception being for UKESM1–0-LL which depicts a SW cooling with an annual mean of −1.8 W/m^2 (Fig. S6b, Table 3). All the models overestimate (underestimate) the SW (LW) cloud radiative warming over CA except UKESM1–0-LL (Fig. S7b, Table 3) which underestimate both SWCRE and LWCRE. IPSL-CM6A-LR exhibits the larger mean bias in SWCRE (5.8 W/m^2) (Table 3), and the larger mean bias in net CRE is recorded for MPI-ESM1–2-LR (−11.9 W/m^2) (Fig. 11d, Fig. S7d) because of it larger mean bias in LWCRE (Fig. S7c), since MPI-ESM1–2-LR does better in simulating the SW CRE over CA with annual mean bias of SWCRE being about 0.7 W/m^2 (Table 3). For MIROC6 and IPSL-CM6A-LR, the positive bias due to overestimation of SW warming partly offset the larger negative bias due to the underestimation of LW warming. Conversely, for UKESM1–0-LL the bias in net CRE results from both the underestimation of LWCRE and SWCRE. Overall, in the atmospheric column, the amplitude of the biases in net CRE are mostly due to larger underestimation of atmospheric LW warming.

At the surface, all the models capture the behavior of the seasonal cycle of SWCRE and net CRE (Fig. S8b,d). The intensity of the radiative effect of clouds significantly differs from one model to another and from model to observation (Fig. 11e). MIROC6 exhibits the larger mean annual value for LW (26.6 W/m^2), SW (−96.1 W/m^2) and net (−69.6 W/m^2) CRE (Fig. S8b-d, Table 3) whereas UKESM1–0-LL exhibits the smaller mean annual value of 5.8 W/m^2, −36.8 W/m and -31 W/m for LW, SW and net CRE respectively. As at the TOA, note that the negative bias in NET, SW (LW) components signifies an overestimation (underestimation) and vice versa. MIROC6 exhibits the larger absolute mean bias in SW (Fig. S9b) and NET (Fig. 11f, Table 3) clouds cooling effect whereas UKESM1–0-LL exhibits the larger absolute mean bias in LW warming (Fig. S9c). MPI-ESM1–2-LR and UKESM1–0-LL underestimate the SW, LW (Fig. S9b, c) and net CRE (Fig. 11f & Fig. S9d) whereas MIROC6 and IPSL-CM6A-LR overestimate the SW (Fig. S9b) and net clouds radiative cooling effect (Fig. 11f, Table 3). All the models underestimate the LW clouds' warming effect with an exception being for MIROC6 which do otherwise. For all the models, the SW mean absolute bias is larger than their LW counterparts. Therefore, the biases in net CRE at the surface are mostly due to the larger bias in SW clouds radiative cooling.

5.3. Spatial distribution and mean bias of TCF

CREs are closely related to cloud fractions (Fig. 6). The maximum of TCF is located between 25°E-30°E (Fig. 12a). All the models fail to capture the geographical distribution of TCF compared to observation (Fig. 12a) with an exemption being for MIROC6 (Fig. 12b). IPSL-CM6A-LR, UKESM1–0-LL and MPI-ESM1–2-LR show their maximum TCF located west of the domain of interest (Fig. 12c-e). All the models capture well the seasonal cycle over CA (Fig. S4a), but with biases in simulating the intensity of the TCF (Fig. S5a) along the seasonal cycle. The investigation of the simulated biases of TCF and CREs in CMIP6 models over CA shows that all the models underestimate the TCF along the seasonal cycle except MIROC6 and MPI-ESM1–2-LR which show a slight (<+5%) overestimation of TCF in April–May and in September–November (Fig. 12f, Fig. S5a). IPSL-CM6A-LR depict the larger annual mean bias of about −14%, UKESM1–0-LL shows an annual mean bias of about −6% whereas MIROC6 and MPI-ESM1–2-LR better simulate the TCF with the annual mean bias <−2%. During the seasonal cycle, IPSL-CM6A-LR exhibits the largest bias of about −25% observed in July–August. It is worth mentioning that the decrease (increase) of TCF bias means the increase (decrease) of TCF in model simulation. The seasonal variation of the TCF bias modulates the seasonal variation of the simulated CREs biases at the TOA (Fig. S5) and at the surface (Fig. S7). For instance, the decreasing (increasing) bias of TCF leads to the increasing (decreasing) bias in SWCRE and the decreasing (increasing) bias in LWCRE, meaning that the TCF is one of the main sources of CREs bias in climate models.

It should be noticed from the section 4.2 analyses, that MIROC6 and IPSL-CM6A-LR overestimate the SW radiative effect at the TOA, in Atmosphere and at the surface, whereas MPI-ESM1–2-LR and UKESM1–0-LL underestimate. It should also be noted that all models underestimate the LWCRE, consistent with the findings over western and eastern Tibetan plateau (Li et al., 2021). Therefore, we gathered those that overestimate the SW radiative effect on one side, and those that underestimate the SW radiative effect on the other side in order to analyze the sensitivity of TCF to SWCRE on both sides. For each of the two groups, we calculated the multimodels ensemble mean for SW, LW at the TOA, in the atmosphere and at the surface. The mean TCF of each of the two groups is also calculated. We denoted by MME1 the multimodels ensemble mean of the models that overestimate the SWCRE and by MME2 for those models which do otherwise. We then performed the correlation between MME1 and MME2 cloud radiative biases and their corresponding TCF biases. The results are presented in Fig. 13. We note at first glance that the correlation between CREs (SW, LW) biases and TCF biases are always high for the two ensembles at the TOA and at the surface. For MME1, whether we are at the TOA in the atmosphere or at the surface, the diminution of the magnitude of TCF biases increases the magnitude of SWCRE bias meaning that the SWCRE increases in the models, but significantly decreases the magnitude of the LWCRE bias at the TOA and in the atmosphere. For MME2, the diminution of the magnitude of TCF bias significantly decreases the magnitude of the SWCRE and LWCRE biases at the TOA, in the atmosphere and at the surface even though the correlation in the atmosphere is not significant. We then conclude that for models with overestimated SW radiation, a better simulated TCF increases the SWCRE bias and ameliorates the simulation of LWCRE. Conversely, for the models with underestimated SWCRE, a good simulation of TCF ameliorates both the simulation of SWCRE and LWCRE. This leads to the conclusion that the underestimation of TCF directly results in the underestimated intensity of LWCRE and SWCRE but is not the only cause of the underestimated SWCRE.

6. Discussion and conclusion

We performed a seasonal analysis of the CRE at the TOA, in the atmosphere and at the surface from CERES data over Central Africa and used it to evaluate CRE in climate models over the same region. Our main motivation to study CRE over Central Africa is that clouds modulate the energy budget, and thus influence the climate, e.g., the atmospheric circulation, sea surface temperature, and the hydrological cycle. Since a poor representation of clouds and their radiative effect in the climate model simulation could bias future climate projections, advancing our understanding of CRE, particularly in an area with high irradiance like Central Africa, is important. The main findings are as follow:

The spatial pattern of the CREs component (shortwave, longwave, net) at the TOA, at the surface and in the atmosphere vary slightly across Central Africa. The reinforcement of the net cloud radiative cooling effect over the West Equatorial Africa is due to large fraction of low stratus clouds during June-to September (Dommo et al., 2018, 2022) which reduces the longwave warming effect and increases the magnitude of the shortwave cooling at the surface during the latter season and then enhances the magnitude of the net cloud cooling effect over West Equatorial Africa (Fig. 1).

The seasonal cycle of the TOA SWCRE and LWCRE over Central Africa is characterized by a bimodal cycle probably in link with the seasonal variation of the sea surface temperature anomalies and the seasonality of high-altitude ice clouds dominating the total cloud fraction. The net effect of clouds at the TOA and at the surface is the cooling whereas, in the atmosphere exhibits a net cloud warming effect. The

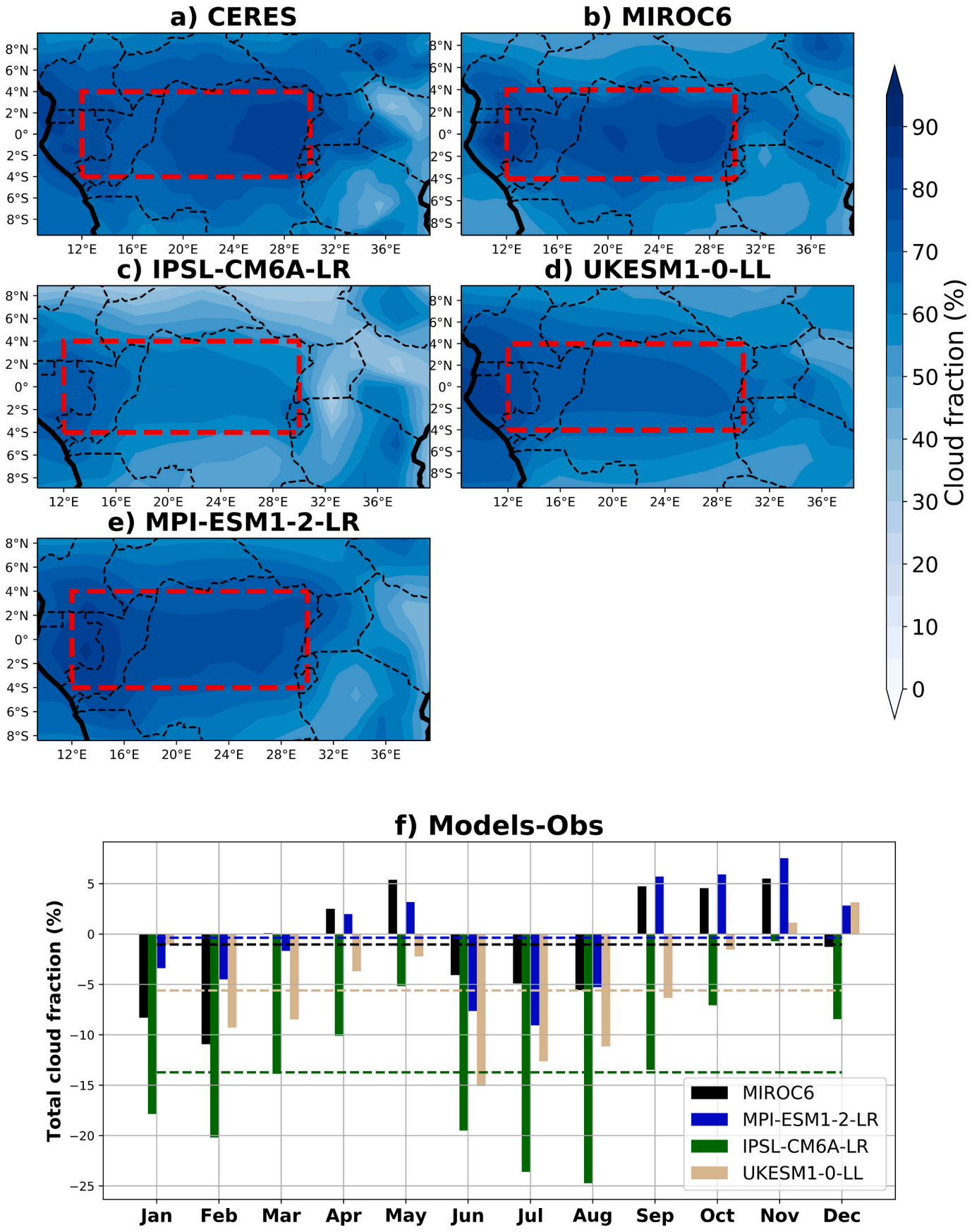

Fig. 12. Spatial distribution (March 2000–December 2014) of the TCF for a) CERES and (b-e) CMIP6 observation. f) Seasonal cycle of the mean bias of TCF between models and observation. To compute the mean bias, data are firstly averaged over 12°E-30°E & 4°S-4°N for the period March 2000–December 2014. The horizontal dashed lines are the annual mean bias for each of the CMIP6 models.

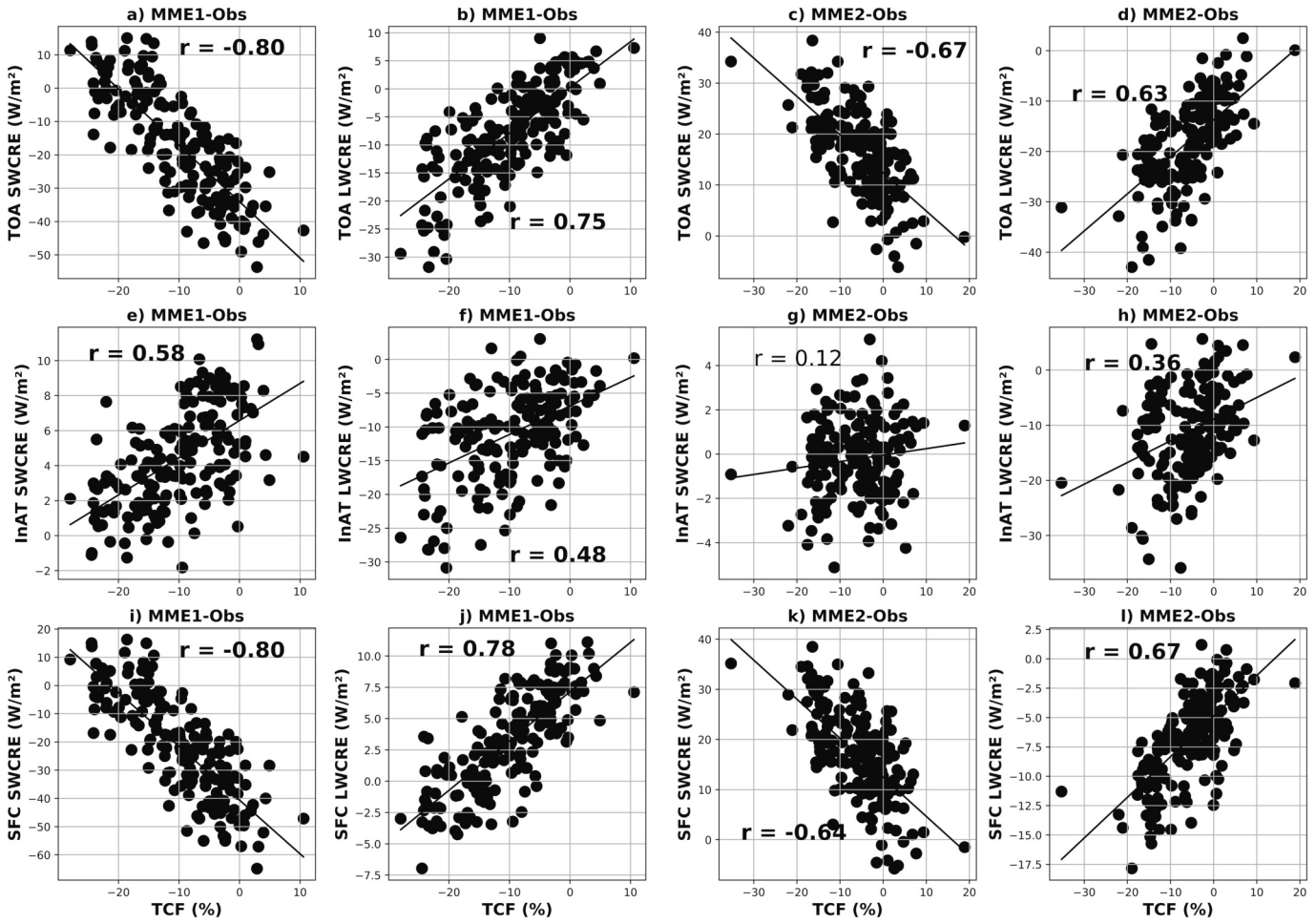

Fig. 13. Scatter plots between the multimodels ensemble SWCRE, LWCRE and TCF at the TOA (first row), in the atmosphere (second row) and at the surface (third row). Each black dot corresponds to the average of each month over the period March 2000–December 2014. The spatial average is performed over 12°E-30°E & 4°S-4°N. Significant Pearson correlation coefficients (r) at two-sided 95% level according to t-test are displayed in bold.

behavior and sign of the net CRE in the atmosphere follow that of the longwave warming, whereas at the surface the behavior and sign of the net CRE follow that of the shortwave cooling.

The comparison of observed CREs with simulated CREs shows that most of the models can capture the effect of clouds on radiation and the spatial pattern of the CREs component (shortwave, longwave, net). At the TOA, all the models can capture the seasonal cycle of the shortwave CRE and longwave CRE (Fig. S4b, c) but not the one of the net CRE (Fig. 11a, Fig. S4d). Conversely, In the atmosphere Fig. S6) and at the surface (Fig. S8), all the models can capture the seasonal cycle of the shortwave, longwave and the net CRE. All the models struggle in simulating the intensity of CREs. At the TOA and at the surface, the absolute values of the magnitudes of biases in shortwave CRE are most of the time larger than the longwave CRE counterpart, whereas in the atmosphere, longwave CRE exhibits the largest biases.

The associated relationship between total cloud fraction and CREs components (longwave, shortwave) shows that cloud biases are not the only cause of SWCRE and LWCRE biases in model simulation. For instance, a better simulated cloud fraction improves the simulation of both SWCRE and LWCRE for models (MPI-ESM1–2-LR, UKESM1–0-LL) that underestimate SWCRE. Conversely, for models (MIROC6, IPSL-CM6A-LR) with overestimated SWCRE, a better simulation of cloud fraction increases the SWCRE bias even though it improves LWCRE simulation. However, to draw a definitive conclusion, this finding should be verified for a large set of CMIP6 models, since only a few were used in this study.

The estimated energy balance over Central Africa at the TOA is −8.4 W/m^2. This value is small compared to the global and tropical average estimated (Table 3), which refers to more energy gain over Central Africa. But the TOA LWCRE and SWCRE are larger compared to the global average (Table 3). At the surface clouds reduce radiation by about −43.9 W/m^2 over Central Africa, more than what is observed in global and tropical averages. While the average energy gain on global average does not exceed 7 W/m^2 in the atmosphere (Wild et al., 2014, 2018), Central Africa exhibits a larger accumulation of energy (35.6 W/m^2) in its atmospheric column. This effect of clouds on radiation will certainly feed the complex atmospheric dynamic circulation over Central Africa. For instance, positive atmospheric CRE were found to (Harrop and Hartmann, 2016; Voigt et al., 2019): strengthen the Hadley circulation, increase the peak of precipitation over the tropic and decrease the tropical mean precipitation. Moreover, in the context of climate sensitivity, CRE plays many important roles including the width of the tropical rain belts, the position of the extratropical storm tracks and the circulation response to global warming (Voigt et al., 2020). Thus, further study on the interconnection between circulation and CREs deserves to be conducted over the region. It has been shown that the measurement of longwave radiation even under clear sky conditions remains a challenge (Kato et al., 2011). Therefore, some of the biases between models and observations could come from the observations themselves. It is noteworthy that as part of this evaluation of CREs in CMIP6 models, a better-simulated cloud fraction does not always lead to a better simulated SWCRE. This implies that the associated relationship between

other cloud parameters and CREs need to be conducted. For instance, Li et al., 2020a,2020b shows that over Southeastern China, most of the models with underestimated cloud liquid water path correspond to their individual weaker SWCRE. Furthermore, as demonstrated in Li et al., 2020a,2020b, a worst simulation of cloud ice water paths can also lead to the underestimation of cloud fraction, and then to a bias in CREs. Additionally, the relationships between surface temperature and surface albedo (Li et al., 2021, 2022), the model's horizontal resolution (Lin and Yu, 2022) may be other sources of CREs biases in CMIP6 models over Central Africa.

Authors contributions

A. DOMMO: Funding acquisition, conceptualization, investigation, data visualization, organization of the paper, software, writing, editing, revision. N.A Browne Klutse: Conceptualization, editing, writing, revison. S. Fiedler: Conceptualization, editing, writing, revision. H. Azoda Koffi: Data curation, editing, revision. DA. Vondou: Data visualization, data curation, editing, revision. All the authors participated to the editing and revision of the work.

Declaration of Competing Interest

The authors declare that they have no known competing financial interests or personal relationships that could have appeared to influence the work reported in this paper.

Data availability

The data used in this study are available on ECMWF website (https://cds.climate.copernicus.eu/cdsapp#!/dataset) for ERA5 reanalysis. The clouds and radiation data can be found at https://ceres.larc.nasa.gov/data/ and CMIP6 data can be downloaded via https://esgf-data.dkrz.de/search/cmip6-dkrz/.

Acknowledgements

This research is supported by DAAD within the framework of the ClimapAfrica programme with funds of the Federal Ministry of Education and Research (funding ID 57610298 and reference 91815194). Authors thank all the data providers used in this study. The first author thanks the University of Ghana for providing the necessary framework for the realization of this work. Authors thank NASA (National Aeronautics and Space Administration) for providing Clouds and the Earth's Radiant Energy System (CERES) Energy Budget and Filled (EBAF) (hereafter, CERES-EBAF) dataset. All the authors are grateful to the ECMWF for providing reanalysis (ERA5) data. We also acknowledge all the CMIP6 data providers, for freely releasing the model's output (https://esgf-data.dkrz.de/search/cmip6-dkrz/). We would also like to express our gratitude to the two anonymous reviewers for their comments that help to significantly increase the quality of the manuscript.

Appendix A. Supplementary data

Supplementary data to this article can be found online at https://doi.org/10.1016/j.atmosres.2023.106820.

References

Allan, R.P., 2011. Combining satellite data and models to estimate cloud radiative effect at the surface and in the atmosphere. Meteorol. Appl. 18 (3), 324–333. https://doi.org/10.1002/met.285.

Baccini, A., Goetz, S.J., Walker, W.S., Laporte, N.T., Sun, M., Sulla-Menashe, D., Hackler, J., Beck, P.S.A., Dubayah, R., Friedl, M.A., Samanta, S., Houghton, R.A., 2012. Estimated carbon dioxide emissions from tropical deforestation improved by carbon-density maps. Nat. Clim. Chang. 2 (3), 182–185. https://doi.org/10.1038/nclimate1354.

Berry, E., Mace, G.G., 2014. Cloud properties and radiative effects of the Asian summer monsoon derived from A-Train data. J. Geophys. Res. Atmos. 119 (15), 9492–9508. https://doi.org/10.1002/2014jd021458.

Birch, C.E., Parker, D.J., Marsham, J.H., Copsey, D., Garcia-Carreras, L., 2014. A seamless assessment of the role of convection in the water cycle of the West African Monsoon. J. Geophys. Res. Atmos. 119 (6), 2890–2912. https://doi.org/10.1002/2013jd020887.

Bony, S., Stevens, B., Frierson, D.M.W., Jakob, C., Kageyama, M., Pincus, R., Shepherd, T. G., Sherwood, S.C., Siebesma, A.P., Sobel, A.H., Watanabe, M., Webb, M.J., 2015. Clouds, circulation and climate sensitivity. Nat. Geosci. 8 (4), 261–268. https://doi.org/10.1038/ngeo2398.

Burleyson, C.D., Long, C.N., Comstock, J.M., 2015. Quantifying diurnal cloud radiative effects by cloud type in the tropical Western Pacific. J. Appl. Meteorol. Climatol. 54 (6), 1297–1312. https://doi.org/10.1175/jamc-d-14-0288.1.

Camberlin, P., Togbedji, C.F., Pergaud, J., Berger, A., Aellig, R., Fink, A.H., Knippertz, P., Moron, V., Philippon, N., 2023. The representation of dry-season low-level clouds over Western Equatorial Africa in reanalyses and historical CMIP6 simulations. Clim. Dyn. https://doi.org/10.1007/s00382-023-06714-w.

Chen, S.S., Houze Jr., R.A., Mapes, B.E., 1996. Multiscale variability of deep convection in realation to large-scale circulation in TOGA COARE. J. Atmos. Sci. 53 (10), 1380–1409. https://doi.org/10.1175/1520-0469(1996)053<1380:mvodci>2.0.co;2.

Chen, T., Rossow, W.B., Zhang, Y., 2000. Radiative effects of cloud-type variations. J. Clim. 13 (1), 264–286. https://doi.org/10.1175/1520-0442(2000)013<0264:reoctv>2.0.co;2.

Collins, W.D., Valero, F.P.J., Flatau, P.J., Lubin, D., Grassl, H., Pilewskie, P., 1996. Radiative effects of convection in the tropical Pacific. J. Geophys. Res. Atmos. 101 (D10), 14999–15012. https://doi.org/10.1029/95jd02534.

Curry, J.A., Schramm, J.L., Rossow, W.B., Randall, D., 1996. Overview of Arctic cloud and radiation characteristics. J. Clim. 9 (8), 1731–1764. https://doi.org/10.1175/1520-0442(1996)009<1731:ooacar>2.0.co;2.

Dargie, G.C., Lewis, S.L., Lawson, I.T., Mitchard, E.T.A., Page, S.E., Bocko, Y.E., Ifo, S.A., 2017. Age, extent and carbon storage of the Central Congo Basin peatland complex. Nature 542 (7639), 86–90. https://doi.org/10.1038/nature21048.

Dommo, A., Philippon, N., Vondou, D.A., Sèze, G., Eastman, R., 2018. The june–september low cloud cover in Western Central Africa: mean spatial distribution and diurnal evolution, and associated atmospheric dynamics. J. Clim. 31 (23), 9585–9603. https://doi.org/10.1175/jcli-d-17-0082.1.

Dommo, A., Vondou, D.A., Philippon, N., Eastman, R., Moron, V., Aloysius, N., 2022. The ERA5's diurnal cycle of low-level clouds over Western Central Africa during June–September: dynamic and thermodynamic processes. Atmos. Res. 280, 106426 https://doi.org/10.1016/j.atmosres.2022.106426.

Eyring, V., Bony, S., Meehl, G.A., Senior, C.A., Stevens, B., Stouffer, R.J., Taylor, K.E., 2016. Overview of the Coupled Model Intercomparison Project Phase 6 (CMIP6) experimental design and organization. Geosci. Model Dev. 9 (5), 1937–1958. https://doi.org/10.5194/gmd-9-1937-2016.

Forster, P., Storelvmo, T., Armour, K., Collins, W., Dufresne, J.L., Frame, D., Lunt, D.J., Mauritsen, T., Palmer, M.D., Watanabe, M., Wild, M., Zhang, H., 2021. The Earth' energy budget, climate feedbacks, and climate sensitivity. In: Masson-Delmotte, V., Zhai, P., Pirani, A., Connors, S.L., Péan, C., Berger, S., Caud, N., Chen, Y., Goldfarb, M., Gomis, I., Huang, M., Leitzell, K., Lonnoy, E., Matthews, J.B.R., Maycock, T.K., Waterfield, T., Yelekçi, O., Yu, R., Zhou, B. (Eds.), Climate Change 2021: The Physical Science Basis. Contribution of Working Group I to the Sixth Assessment Report of the Intergovernmental Panel on Climate Change. Cambridge University Press. In Press.

Furtado, K., Field, P.R., Boutle, I.A., Morcrette, C.J., Wilkinson, J.M., 2015. A physically based subgrid parameterization for the production and maintenance of mixed-phase clouds in a general circulation model. J. Atmos. Sci. 73 (1), 279–291. https://doi.org/10.1175/jas-d-15-0021.1.

Garrett, T., Zhao, C., 2006. Increased Arctic cloud longwave emissivity associated with pollution from mid-latitudes. Nature 440, 787–789. https://doi.org/10.1038/nature04636.

Harrison, E.F., Minnis, P., Barkstrom, B.R., Ramanathan, V., Cess, R.D., Gibson, G.G., 1990. Seasonal variation of cloud radiative forcing derived from the Earth Radiation Budget Experiment. J. Geophys. Res. 95 (D11), 18687. https://doi.org/10.1029/jd095id11p18687.

Harrop, B.E., Hartmann, D.L., 2016. The role of cloud radiative heating in determining the location of the ITCZ in aquaplanet simulations. J. Clim. 29 (8), 2741–2763. https://doi.org/10.1175/jcli-d-15-0521.1.

Hartmann, D.L., Ockert-Bell, M.E., Michelsen, M.L., 1992. The effect of cloud type on Earth's energy balance: global analysis. J. Clim. 5 (11), 1281–1304. https://doi.org/10.1175/1520-0442(1992)005<1281:teocto>2.0.co;2.

Hartmann, D.L., Moy, L.A., Fu, Q., 2001. Tropical convection and the energy balance at the top of the atmosphere. J. Clim. 14 (24), 4495–4511. https://doi.org/10.1175/1520-0442(2001)014<4495:tcateb>2.0.co;2.

Henderson, D.S., L'Ecuyer, T., Stephens, G., Partain, P., Sekiguchi, M., 2013. A multisensor perspective on the radiative impacts of clouds and aerosols. J. Appl. Meteorol. Climatol. 52 (4), 853–871. https://doi.org/10.1175/jamc-d-12-025.1.

Hersbach, H., Bell, B., Berrisford, P., Hirahara, S., Horanyi, A., Muñoz-Sabater, J., Nicolas, J., Peubey, C., Radu, R., Schepers, D., Simmons, A., Soci, C., Abdalla, S., Abellan, X., Balsamo, G., Bechtold, P., Biavati, G., Bidlot, J., Bonavita, M., de Chiara, G., Dahlgren, P., Dee, D., Diamantakis, M., Dragani, R., Flemming, J., Forbes, R., Fuentes, M., Geer, A., Haimberger, L., Healy, S., Hogan, R.J., Holm, E., Janiskova, M., Keeley, S., Laloyaux, P., Lopez, P., Lupu, C., Radnoti, G., de Rosnay, P., Rozum, I., Vamborg, F., Villaume, S., Thépaut, J.N., 2020. The ERA5 global reanalysis. Q. J. R. Meterol. Soc. 146 (730), 1999–2049.

Hill, P.G., Allan, R.P., Chiu, J.C., Stein, T.H.M., 2016. A multisatellite climatology of clouds, radiation, and precipitation in southern West Africa and comparison to climate models. J. Geophys. Res. Atmos. 121 (18), 10,857–10,879. https://doi.org/10.1002/2016jd025246.

Hill, P.G., Allan, R.P., Chiu, J.C., Bodas-Salcedo, A., Knippertz, P., 2018. Quantifying the contribution of different cloud types to the radiation budget in Southern West Africa. J. Clim. 31 (13), 5273–5291. https://doi.org/10.1175/jcli-d-17-0586.1.

Jiang, J.H., Su, H., Zhai, C., Watanabe, M., 2013. Correction to "Evaluation of cloud and water vapor simulations in CMIP5 climate models using NASA 'A-Train' satellite observations.". J. Geophys. Res. Atmos. 118 (19), 11,087. https://doi.org/10.1002/jgrd.50864.

Jiang, S., Zhao, C., Xia, Y., 2022. Distinct response of near surface air temperature to clouds in North China. Atmos. Sci. Lett. 23 (12), e1128 https://doi.org/10.1002/asl.1128JIANGET. AL.7of7.

Johnson, R.H., Rickenbach, T.M., Rutledge, S.A., Ciesielski, P.E., Schubert, W.H., 1999. Trimodal characteristics of tropical convection. J. Clim. 12 (8), 2397–2418. https://doi.org/10.1175/1520-0442(1999)012<2397:tcotc>2.0.co;2.

Kato, S., Rose, F.G., Sun-Mack, S., Miller, W.F., Chen, Y., Rutan, D.A., Stephens, G.L., Loeb, N.G., Minnis, P., Wielicki, B.A., Winker, D.M., Charlock, T.P., Stackhouse Jr., P.W., Xu, K.-M., Collins, W.D., 2011. Improvements of top-of-atmosphere and surface irradiance computations with CALIPSO-, CloudSat-, and MODIS-derived cloud and aerosol properties. J. Geophys. Res. 116 (D19) https://doi.org/10.1029/2011jd016050.

Kato, S., Loeb, N.G., Rose, F.G., Doelling, D.R., Rutan, D.A., Caldwell, T.E., Yu, L., Weller, R.A., 2013. Surface irradiances consistent with ceres-derived top-of-atmosphere shortwave and longwave irradiances. J. Clim. 26 (9), 2719–2740. https://doi.org/10.1175/jcli-d-12-00436.1.

Kato, S., Rose, F.G., Rutan, D.A., Thorsen, T.J., Loeb, N.G., Doelling, D.R., Huang, X., Smith, W.L., Su, W., Ham, S.-H., 2018. Surface irradiances of edition 4.0 Clouds and the earth's radiant energy system (CERES) energy balanced and filled (EBAF) data product. J. Clim. 31 (11), 4501–4527. https://doi.org/10.1175/jcli-d-17-0523.1.

Kay, J.E., Wall, C., Yettella, V., Medeiros, B., Hannay, C., Caldwell, P., Bitz, C., 2016. Global climate impacts of fixing the Southern Ocean shortwave radiation bias in the community earth system model (CESM). J. Clim. 29 (12), 4617–4636. https://doi.org/10.1175/jcli-d-15-0358.1.

Kuete, G., Pokam Mba, W., Washington, R., 2019. African Easterly Jet South: control, maintenance mechanisms and link with Southern subtropical waves. Clim. Dyn. 54 (3–4), 1539–1552. https://doi.org/10.1007/s00382-019-05072-w.

Kuete, G., Mba, W.P., James, R., Dyer, E., Annor, T., Washington, R., 2022. How do coupled models represent the African Easterly Jets and their associated dynamics over Central Africa during the September–November rainy season? Clim. Dyn. https://doi.org/10.1007/s00382-022-06467-y.

Lauer, A., Hamilton, K., 2013. Simulating clouds with global climate models: a comparison of CMIP5 results with CMIP3 and satellite data. J. Clim. 26 (11), 3823–3845. https://doi.org/10.1175/jcli-d-12-00451.1.

L'Ecuyer, T.S., Hang, Y., Matus, A.V., Wang, Z., 2019. Reassessing the effect of cloud type on Earth's energy balance in the age of active spaceborne observations. Part I: top of atmosphere and surface. J. Clim. 32 (19), 6197–6217. https://doi.org/10.1175/jcli-d-18-0753.1.

Li, J.-L.F., Waliser, D.E., Stephens, G., Lee, S., L'Ecuyer, T., Kato, S., Loeb, N., Ma, H.-Y., 2013. Characterizing and understanding radiation budget biases in CMIP3/CMIP5 GCMs, contemporary GCM, and reanalysis. J. Geophys. Res. Atmos. 118 (15), 8166–8184. https://doi.org/10.1002/jgrd.50378.

Li, R., Jin, J., Wang, S.-Y., Gillies, R.R., 2014. Significant impacts of radiation physics in the weather research and forecasting model on the precipitation and dynamics of the West African Monsoon. Clim. Dyn. 44 (5–6), 1583–1594. https://doi.org/10.1007/s00382-014-2294-2.

Li, Jiandong, Wang, W.-C., Dong, X., Mao, J., 2017. Cloud-radiation-precipitation associations over the Asian monsoon region: an observational analysis. Clim. Dyn. 49 (9–10), 3237–3255. https://doi.org/10.1007/s00382-016-3509-5.

Li, Y., Thompson, D.W.J., Olonscheck, D., 2020a. A basic effect of cloud radiative effects on tropical sea surface temperature variability. J. Clim. 33 (10), 4333–4346. https://doi.org/10.1175/jcli-d-19-0298.1.

Li, J., You, Q., He, B., 2020b. Distinctive spring shortwave cloud radiative effect and its inter-annual variation over southeastern China. Atmos. Sci. Lett. 21 (6) https://doi.org/10.1002/asl.970.

Li, J., Sun, Z., Liu, Y., You, Q., Chen, G., Bao, Q., 2021. Top-of-Atmosphere Radiation Budget and Cloud Radiative Effects over the Tibetan Plateau and Adjacent Monsoon Regions from CMIP6 Simulations. Wiley. https://doi.org/10.1002/essoar.10505197.1.

Li, J., Wang, W.-C., Chen, G., You, Q., 2022. Characteristics of top-of-atmosphere radiation budget over the Tibetan Plateau and its bias sources in climate models. Atmos. Res. 276, 106256 https://doi.org/10.1016/j.atmosres.2022.106256.

Lin, Q.-J., Yu, J.-Y., 2022. The potential impact of model horizontal resolution on the simulation of atmospheric cloud radiative effect in CMIP6 models. TAO. 33 (1) https://doi.org/10.1007/s44195-022-00021-3.

Liou, K.-N., 1992. Radiation and Cloud Processes in the Atmosphere: Theory, Observation and Modeling. Oxford University Press on Demand.

Loeb, N.G., Doelling, D.R., Wang, H., Su, W., Nguyen, C., Corbett, J.G., Liang, L., Mitrescu, C., Rose, F.G., Kato, S., 2018. Clouds and the earth's radiant energy system (CERES) energy balanced and filled (EBAF) top-of-atmosphere (TOA) edition-4.0 Data product. J. Clim. 31 (2), 895–918. https://doi.org/10.1175/jcli-d-17-0208.1.

Loeb, N.G., Rose, F.G., Kato, S., Rutan, D.A., Su, W., Wang, H., Doelling, D.R., Smith, W. L., Gettelman, A., 2020. Toward a consistent definition between satellite and model clear-sky radiative fluxes. J. Clim. 33 (1), 61–75. https://doi.org/10.1175/jcli-d-19-0381.1.

Marsham, J.H., Dixon, N.S., Garcia-Carreras, L., Lister, G.M.S., Parker, D.J., Knippertz, P., Birch, C.E., 2013. The role of moist convection in the West African monsoon system: insights from continental-scale convection-permitting simulations. Geophys. Res. Lett. 40 (9), 1843–1849. https://doi.org/10.1002/grl.50347.

Moihamette, F., Pokam, W.M., Diallo, I., Washington, R., 2022. Extreme Indian Ocean dipole and rainfall variability over Central Africa. Int. J. Climatol. 42 (10), 5255–5272. https://doi.org/10.1002/joc.7531.

Myhre, G., Samset, B.H., Schulz, M., Balkanski, Y., Bauer, S., Berntsen, T.K., Bian, H., Bellouin, N., Chin, M., Diehl, T., Easter, R.C., Feichter, J., Ghan, S.J., Hauglustaine, D., Iversen, T., Kinne, S., Kirkevåg, A., Lamarque, J.-F., Lin, G., Zhou, C., 2012. Radiative forcing of the direct aerosol effect from AeroCom phase II simulations. Copernicus GmbH. https://doi.org/10.5194/acpd-12-22355-2012.

Peixoto, J.P., 1992. Physics of Climate. Springer.

Pokam, W.M., Djiotang, L.A.T., Mkankam, F.K., 2011. Atmospheric water vapor transport and recycling in Equatorial Central Africa through NCEP/NCAR reanalysis data. Clim. Dyn. 38 (9–10), 1715–1729. https://doi.org/10.1007/s00382-011-1242-7.

Pokam, W.M., Bain, C.L., Chadwick, R.S., Graham, R., Sonwa, D.J., Kamga, F.M., 2014. Identification of processes driving low-level westerlies in West Equatorial Africa. J. Clim. 27 (11), 4245–4262. https://doi.org/10.1175/jcli-d-13-00490.1.

Prata, A.J., 1996. A new long-wave formula for estimating downward clear-sky radiation at the surface. Q. J. R. Meteorol. Soc. 122 (533), 1127–1151. https://doi.org/10.1002/qj.49712253306.

Ramanathan, V., Cess, R.D., Harrison, E.F., Minnis, P., Barkstrom, B.R., Ahmad, E., Hartmann, D., 1989. Cloud-Radiative forcing and climate: results from the earth radiation budget experiment. Science 243 (4887), 57–63. https://doi.org/10.1126/science.243.4887.57.

Rodwell, M.J., Jung, T., 2008. Understanding the local and global impacts of model physics changes: an aerosol example. Q. J. R. Meteorol. Soc. 134 (635), 1479–1497. https://doi.org/10.1002/qj.298.

Rossow, W.B., Zhang, Y.-C., 1995. Calculation of surface and top of atmosphere radiative fluxes from physical quantities based on ISCCP data sets: 2. Validation and first results. J. Geophys. Res. Atmos. 100 (D1), 1167–1197. https://doi.org/10.1029/94jd02746.

Rutan, D., Rose, F., Roman, M., Manalo-Smith, N., Schaaf, C., Charlock, T., 2009. Development and assessment of broadband surface albedo from Clouds and the Earth's Radiant Energy System Clouds and Radiation Swath data product. J. Geophys. Res. 114 (D8) https://doi.org/10.1029/2008jd010669.

Schulz, M., Textor, C., Kinne, S., Balkanski, Y., Bauer, S., Berntsen, T., Berglen, T., Boucher, O., Dentener, F., Guibert, S., Isaksen, I.S.A., Iversen, T., Koch, D., Kirkevåg, A., Liu, X., Montanaro, V., Myhre, G., Penner, J.E., Pitari, G., Takemura, T., 2006. Radiative forcing by aerosols as derived from the AeroCom present-day and pre-industrial simulations. Atmos. Chem. Phys. 6 (12), 5225–5246. https://doi.org/10.5194/acp-6-5225-2006.

Shupe, M.D., Intrieri, J.M., 2004. Cloud radiative forcing of the arctic surface: the influence of cloud properties, surface albedo, and solar zenith angle. J. Clim. 17 (3), 616–628. https://doi.org/10.1175/1520-0442(2004)017<0616:crfota>2.0.co;2.

Slingo, A., Slingo, J.M., 1988. The response of a general circulation model to cloud longwave radiative forcing. I: introduction and initial experiments. Q. J. R. Meteorol. Soc. 114 (482), 1027–1062. https://doi.org/10.1002/qj.49711448209.

Stephens, G.L., Webster, P.J., 1981. Clouds and climate: sensitivity of simple systems. J. Atmos. Sci. 38 (2), 235–247. https://doi.org/10.1175/1520-0469(1981)038<0235:cacsos>2.0.co;2.

Stephens, G.L., Li, J., Wild, M., Clayson, C.A., Loeb, N., Kato, S., L'Ecuyer, T., Stackhouse Jr., P.W., Lebsock, M., Andrews, T., 2012. An update on Earth's energy balance in light of the latest global observations. Nat. Geosci. 5 (10), 691–696. https://doi.org/10.1038/ngeo1580.

Su, W., Corbett, J., Eitzen, Z., Liang, L., 2015. Next-generation angular distribution models for top-of-atmosphere radiative flux calculation from CERES instruments: methodology. Atmos. Meas. Tech. 8 (2), 611–632. https://doi.org/10.5194/amt-3-611-2015.

Taguela, T.N., Vondou, D.A., Moufouma-Okia, W., Fotso-Nguemo, T.C., Pokam, W.M., Tanessong, R.S., Yepdo, Z.D., Haensler, A., Longandjo, G.N., Bell, J.P., Takong, R.R., Djiotang Tchotchou, L.A., 2020. CORDEX multi-rcm hindcast over Central Africa: evaluation within observational uncertainty. J. Geophys. Res. Atmos. 125 (5) https://doi.org/10.1029/2019jd031607.

Taguela, T.N., Pokam, W.M., Washington, R., 2022a. Rainfall in uncoupled and coupled versions of the Met Office Unified Model over Central Africa: investigation of processes during the September–November rainy season. Int. J. Climatol. 42 (12), 6311–6331. https://doi.org/10.1002/joc.7591.

Taguela, T.N., Pokam, W.M., Dyer, E., James, R., Washington, R., 2022b. Low-level circulation over Central Equatorial Africa as simulated from CMIP5 to CMIP6 models. Clim. Dyn. https://doi.org/10.1007/s00382-022-06411-0.

Tamoffo, A.T., Nikulin, G., Vondou, D.A., Dosio, A., Nouayou, R., Wu, M., Igri, P.M., 2021. Process-based assessment of the impact of reduced turbulent mixing on Congo Basin precipitation in the RCA4 Regional Climate Model. Clim. Dyn. 56 (5–6), 1951–1965. https://doi.org/10.1007/s00382-020-05571-1.

Tamoffo, A.T., Amekudzi, L.K., Weber, T., Vondou, D.A., Yamba, E.I., Jacob, D., 2022. Mechanisms of rainfall biases in two CORDEX-CORE regional climate models at rainfall peaks over Central Equatorial Africa. J. Clim. 35 (2), 639–668. https://doi.org/10.1175/jcli-d-21-0487.1.

Tompkins, A.M., 2005. Influence of aerosol climatology on forecasts of the African Easterly Jet. Geophys. Res. Lett. 32 (10) https://doi.org/10.1029/2004gl022189.

Voigt, A., Albern, N., Papavasileiou, G., 2019. The atmospheric pathway of the cloud-radiative impact on the circulation response to global warming: important and uncertain. J. Clim. 32 (10), 3051–3067. https://doi.org/10.1175/jcli-d-18-0810.1.

Voigt, A., Albern, N., Ceppi, P., Grise, K., Li, Y., Medeiros, B., 2020. Clouds, radiation, and atmospheric circulation in the present-day climate and under climate change. WIREs Clim. Chang. 12 (2) https://doi.org/10.1002/wcc.694.

Wang, J., Jian, B., Wang, G., Zhao, Y., Li, Y., Letu, H., Zhang, M., Li, J., 2021. Climatology of cloud phase, cloud radiative effects and precipitation properties over the Tibetan Plateau. Remote Sens. 13 (3), 363. https://doi.org/10.3390/rs13030363.

Watt-Meyer, O., Frierson, D.M.W., 2017. Local and remote impacts of atmospheric cloud radiative effects onto the eddy-driven jet. Geophys. Res. Lett. 44 (19) https://doi.org/10.1002/2017gl074901.

Wild, M., 2012a. Enlightening global dimming and brightening. BAMS 93 (1), 27–37. https://doi.org/10.1175/bams-d-11-00074.1.

Wild, M., 2012b. New Directions: a facelift for the picture of the global energy balance. Atmos. Environ. 55, 366–367. https://doi.org/10.1016/j.atmosenv.2012.03.022.

Wild, M., 2020. The global energy balance as represented in CMIP6 climate models. Clim. Dyn. 55 (3–4), 553–577. https://doi.org/10.1007/s00382-020-05282-7.

Wild, M., Folini, D., Schär, C., Loeb, N., Dutton, E.G., König-Langlo, G., 2012. The global energy balance from a surface perspective. Clim. Dyn. 40 (11–12), 3107–3134. https://doi.org/10.1007/s00382-012-1569-8.

Wild, M., Folini, D., Hakuba, M.Z., Schär, C., Seneviratne, S.I., Kato, S., Rutan, D., Ammann, C., Wood, E.F., König-Langlo, G., 2014. The energy balance over land and oceans: an assessment based on direct observations and CMIP5 climate models. Clim. Dyn. 44 (11−12), 3393–3429. https://doi.org/10.1007/s00382-014-2430-z.

Wild, M., Hakuba, M.Z., Folini, D., Dörig-Ott, P., Schär, C., Kato, S., Long, C.N., 2018. The cloud-free global energy balance and inferred cloud radiative effects: an assessment based on direct observations and climate models. Clim. Dyn. 52 (7–8), 4787–4812. https://doi.org/10.1007/s00382-018-4413-y.

Xia, Y., Hu, Y., Hu, Y., Zhao, C., Xie, F., Yang, Y., 2021a. Significant contribution of severe ozone loss to the Siberian-Arctic surface warming in Spring 2020. Geophys. Res. Lett. 48 https://doi.org/10.1029/2021GL092509.

Xia, Y., Zhao, Chuanfeng, Hu, Yongyun, Huang, Yi, Bian, Jianchun, 2021b. Stratospheric ozone loss-induced cloud effects lead to less surface ultraviolet radiation over the Siberian Arctic in spring. Environ. Res. Lett. 16 (8), 8. https://doi.org/10.1088/1748-9326/ac18e9.

Xie, S., Liu, X., Zhao, C., Zhang, Y., 2013. Sensitivity of CAM5-simulated Arctic clouds and radiation to ice nucleation parameterization. J. Clim. 26, 5981–5999. https://doi.org/10.1175/JCLI-D-12-00517.1.

Xie, T., Li, J., Sun, C., Ding, R., Wang, K., Zhao, C., Feng, J., 2019. NAO implicated as a predictor of the surface air temperature multidecadal variability over East Asia. Clim. Dyn. 53, 895–905. https://doi.org/10.1007/s00382-019-04624-4.

Zhang, Haotian, Zhao, Chuanfeng, Xia, Yan, Yang, Yikun, 2023. North Atlantic oscillation associated variation in cloud phase and cloud radiative forcing over the Greenland Ice Sheet. J. Clim. 36, 1–37. https://doi.org/10.1175/JCLI-D-22-0718.1.

Zhao, C., Garrett, T.J., 2015. Effects of Arctic haze on surface cloud radiative forcing. Geophys. Res. Lett. 42, 557–564. https://doi.org/10.1002/2014GL062015.

Zhao, L., Wang, Y., Zhao, C., Dong, X., Yung, Y.L., 2022. Compensating errors in cloud radiative and physical properties over the Southern Ocean in the CMIP6 climate models. Adv. Atmos. Sci. 39 (12), 2156–2171. https://doi.org/10.1007/s00376-022-2036-z.